c.2

RESEARCH MEMORANDUM

APPLICATION OF AREA SUCTION TO LEADING-EDGE AND TRAILING-EDGE FLAPS ON A 44° SWEPT-WING MODEL

By Curt A. Holzhauser, Robert K. Martin,
and V. Robert Page

Ames Aeronautical Laboratory
Moffett Field, Calif.

NATIONAL ADVISORY COMMITTEE
FOR AERONAUTICS

WASHINGTON

September 26, 1956

NACA RM A56F01

NATIONAL ADVISORY COMMITTEE FOR AERONAUTICS

RESEARCH MEMORANDUM

APPLICATION OF AREA SUCTION TO LEADING-EDGE AND TRAILING-EDGE FLAPS ON A 44° SWEPT-WING MODEL

By Curt A. Holzhauser, Robert K. Martin, and V. Robert Page

SUMMARY

A wind-tunnel investigation was conducted with a 44° swept-wing model to determine the effects leading- and trailing-edge area-suction flaps have on the static longitudinal characteristics of this model, and to measure the suction requirements of the flaps.

The first portion of the investigation was directed toward determining the lift increments and suction requirements of the trailing-edge area-suction flaps. These tests were made with a normal wing leading edge (undeflected nose flap), and they showed that area suction applied to the trailing-edge flap increased the flap lift increments up to the maximum lift coefficient. It was found that the changes in the force characteristics and the suction requirements for the trailing-edge area-suction flaps could be estimated for 0° angle of attack by the use of methods set forth in previous reports.

The second portion of the investigation was made with a leading-edge flap deflected 40° and with several configurations of the trailing-edge flap. These tests showed that applying area suction at the knee of the leading-edge flap delayed leading-edge air-flow separation and increased the maximum lift coefficient from 1.4 to 2.0 for the model with the area-suction trailing-edge flap deflected.

INTRODUCTION

The use of area suction as a method of increasing the maximum lift coefficients of swept wings has been the subject of numerous studies and investigations. Area suction in its early applications to swept wings was employed to delay leading-edge type of air-flow separation. The

results of tests in which area suction was applied near the leading edge of the wing or on the knee of a leading-edge flap are reported in references 1 through 5. In each of these cases, leading-edge separation was delayed to a higher angle of attack and the maximum lift coefficient was increased. Investigations with area suction applied only to the knee of the trailing-edge flap are reported in references 6 through 9. By the application of suction to the trailing-edge flap the flow remained attached on the flap to high flap deflections and the lift coefficients were increased at a given angle of attack; however, the increases in the maximum lift coefficients were small because leading-edge separation occurred at a reduced angle of attack. To further increase the maximum lift coefficients of swept wings having high-lift trailing-edge flaps, it was found necessary to also delay leading-edge separation. The results of investigations in which both the leading-edge separation and that on the trailing-edge flap were delayed by area suction are reported in references 4, 6, and 9. In reference 6 a method was presented whereby the lift increments and flow requirements could be estimated for trailing-edge area-suction flaps on different wing plan forms.

The present investigation was made with a model which had a wing swept back 44°, an aspect ratio of 3.74, and a taper ratio of 0.40. This investigation had two objectives. The first objective was to determine the effects of a trailing-edge area-suction flap on the force characteristics of the model and to compare these results and the suction requirements with those predicted by the method of reference 6. The second objective was to determine the effects a leading-edge area-suction flap had on the force characteristics of the model with and without a trailing-edge flap.

The present investigation consisted of two phases. The first phase was a study of the trailing-edge flap with an undeflected leading-edge flap. The trailing-edge flap was tested with numerous chordwise porous-area openings, using two spanwise extents of flap at various deflections. The second phase was a study with the leading-edge flap deflected 40° and with several trailing-edge-flap configurations. For selected configurations, the horizontal tail was then added to establish its effect upon the force characteristics of the model.

NOTATION

B.L. boundary layer

b wing span, ft

c chord of wing, ft

$\bar{c}$ mean aerodynamic chord, $\frac{\int_0^{b/2} c^2 dy}{\int_0^{b/2} c\, dy}$, ft

C_D drag coefficient, $\frac{\text{drag}}{qS}$

ΔC_D increase in drag coefficient when trailing-edge flap was deflected at 0° angle of attack

c_l section lift coefficient, $\frac{1}{c}\oint P\, dx \cos\alpha - \frac{1}{c}\oint P\, dz \sin\alpha$

C_L lift coefficient, $\frac{\text{lift}}{qS}$

$C_{L_{\delta_1}}$ rate of change of lift increment per unit deflection of a full wing-chord flap

ΔC_{L_F} increase in lift coefficient when trailing-edge flap was deflected at 0° angle of attack

C_m pitching-moment coefficient referred to quarter-chord point of mean aerodynamic chord, $\frac{\text{pitching moment}}{q\bar{c}S}$

ΔC_m increase in pitching-moment coefficient when trailing-edge flap was deflected at 0° angle of attack

C_Q flow coefficient, $\frac{Q}{US}$

L.E. leading edge

p free-stream static pressure, lb/sq ft

p_d average duct static pressure, lb/sq ft

p_l local static pressure, lb/sq ft

Δp pressure drop across porous material, lb/sq ft

P airfoil surface pressure coefficient, $\frac{p_l - p}{q}$

P_d	average duct pressure coefficient, $\frac{p_d - p}{q}$
q	free-stream dynamic pressure, lb/sq ft
Q	volume of air removed through porous area, corrected to standard sea-level conditions, cu ft/sec
S	wing area, sq ft
T.E.	trailing edge
t	thickness of porous material, in.
U	free-stream velocity, ft/sec
w	average suction air velocity, ft/sec
x	chordwise distance, ft
y	spanwise distance, ft
z	vertical ordinate of airfoil referred to mean camber line of unflapped airfoil, ft
α	angle of attack referred to fuselage center line, deg
δ	flap deflection measured in a plane perpendicular to flap hinge line, deg
$\frac{d\alpha}{d\delta}$	lift effectiveness parameter, $\frac{C_{L_\delta}}{C_{L_\alpha}}$
η	fraction of wing semispan, $\frac{2y}{b}$
Λ	sweep angle, deg

Subscripts

F	trailing-edge flap
N	leading-edge flap
crit	critical
max	maximum

MODEL AND APPARATUS

Photographs of the model in the Ames 40- by 80-foot wind tunnel and the geometry of the model are presented in figure 1 and 2, respectively.

The wing panels of the model (fig. 2(b)) were, with a few modifications, the same as those used in reference 4. A wedge was added at the root to increase the sweep of the quarter-chord line to 44°. The plan form used had an aspect ratio of 3.74 and a taper ratio of 0.4. The maximum thickness of the wing was about 11 percent of the chord measured in a plane perpendicular to the quarter-chord line; the coordinates of the airfoil section are given in table I. Surface pressure orifices were located at the four spanwise stations shown in figure 2(b), and their chordwise positions are listed in table II. The wing was constructed with two spanwise extents of trailing-edge flap and a full-span leading-edge flap.

A cross-sectional view of the trailing-edge flap is shown in figure 2(c). A solid insert was used for the undeflected flap and porous inserts were used for the 50°, 61°, and 66° deflections. Most of these porous inserts were constructed of electroplated screen with a felt backing of a constant 1/16-inch thickness. The porous screen was 0.008 inch thick, with 4225 holes per square inch and had approximately 11-percent open area. The flow characteristics of the porous screen with the 1/16-inch felt backing, as calibrated in a duct, are given in figure 3. An additional insert for the short-span (η_F = 0.16 to 0.50) 61° flap deflection was made of 0.05-inch-thick, porous stainless steel with the chordwise pressure drop variation as shown in figure 4. The extent of porous area for all flap configurations was controlled by sealing all or a portion of the porous surface with a nonporous tape about 0.003 inch thick. The reference line for the various porous-area openings of the deflected trailing-edge flaps was the midpoint of an arc of the respective flap deflection. (Note in figure 2(c) that the circular arc is measured between the points of tangency to the wing surface.)

The leading-edge flap was deflected 40°, and the porous material insert was constructed like those used for the trailing-edge flap. Two designs of porous inserts were tested; one insert had a 1/16-inch constant thickness felt backing with the flow characteristics shown in figure 3. The other insert was made of a tapered wool felt backing cut from 1/2-inch-thick hard wool felt. The flow characteristics of the 1/2-inch-thick felt, as calibrated in a duct, are shown in figure 3. Flow measurements indicated that the pressure drop for a given inflow velocity was proportional to the thickness of the felt. The distributions of thickness used on the leading-edge flap are shown in figure 5 and are the same as those tested in reference 4.

The fuselage had a circular cross section, with a maximum radius of 0.14 semispan, and a fineness ratio of 11.6. Coordinates for the fuselage are listed in table III. The wing panels were mounted on this fuselage in a midwing location.

The horizontal tail used was swept back 45° at the quarter chord, had an aspect ratio of 3.57, and a taper ratio of 0.27. The distance between wing and tail quarter-chord lines, at their intersection with the mean aerodynamic chord, was 1.49 wing mean aerodynamic chord lengths. The horizontal tail was mounted on the center line of the fuselage.

The vertical tail was swept back 44° at the quarter-chord line, had an aspect ratio of 1.87, and a taper ratio of 0.40. Both the vertical and horizontal tail had NACA 64A010 airfoil sections normal to their quarter-chord lines.

The suction equipment was housed in the fuselage and consisted of a separate and independent system for the leading- and trailing-edge flaps. Each system used a centrifugal compressor, driven by a variable-speed electric motor, to take air from the porous area, through a duct, to a plenum chamber in the fuselage, and then to the free stream by an exit duct, located under the fuselage. At this point of exit, survey rakes were used to determine the quantity of flow. The rakes had been calibrated with a standard ASME orifice meter.

TEST AND PROCEDURE

In previous applications of area suction on flaps (refs. 4 and 6 through 9), it was found that, at a given angle of attack below $C_{L_{max}}$, an abrupt increase in lift coefficient was measured with a small increase of flow coefficient. The sketch illustrates a typical variation of lift coefficient with suction flow coefficient. In the present investigation, the critical point and its accompanying suction requirement were determined for each flap configuration by varying the pump speed at a fixed angle of attack. The results of applying suction for both leading- and trailing-edge flaps of the present test were similar to those described in references 4 and 6, in that a critical point could be determined for all configurations from the force data. (This was not the case for the results of reference 9.) Tuft studies indicated that for some configurations, separation

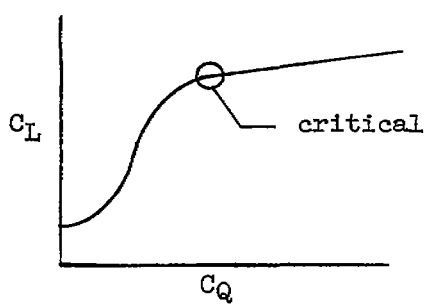

was not entirely eliminated at the critical point. For these configurations, separation could not be eliminated even with the maximum flow coefficients available. The critical flow condition thus having been established, polars were then run for selected configurations with the flow coefficients above $C_{Q_{crit}}$.

Three-component force data and wing pressure measurements were taken for all configurations. Data were also taken of the duct pressures, plenum chamber pressures, and quantities of flow requirements for all applications of the suction flaps.

The porous-area openings tested on the various suction flaps are listed in table IV. Table V gives the various model configurations, their accompanying free-stream velocity, and the number of the figure where the data are presented.

The free-stream velocities of 156 and 202 feet per second that were used in this test corresponded to Reynolds numbers of 10.3×10^6 and 13.1×10^6, respectively. For these tests, the model was held at 0° angle of sideslip, while the angle of attack was varied from -8° to 30°.

CORRECTIONS

The standard tunnel-wall corrections for a straight wing of the same area and span as the sweptback wing were applied to the angle of attack, pitching-moment coefficient, and drag coefficient data. The increments that were added to the data are as follows:

$$\Delta\alpha = 0.74\ C_L$$
$$\Delta C_D = 0.0129\ C_L^2$$
$$\Delta C_m = 0.0084\ C_L \quad \text{(tail-on data only)}$$

No corrections were made for the drag of the exposed portion of the lift strut and its interference with the wing. The limited data available indicate this drag coefficient to vary from 0.003 at a lift coefficient of 0 to 0 at 30° angle of attack.

All values of flow coefficient were corrected for leakage and they were also corrected to standard sea-level conditions. The effect of the exhausting jets on the aerodynamic characteristics was found to be negligible.

RESULTS AND DISCUSSION

Model With Undeflected Leading-Edge Flap and Without a Horizontal Tail

The lift, drag, and moment data in figure 6 are presented to show how the characteristics of the wing were affected when the trailing-edge flap was deflected and area suction was applied at the knee of the flap. These figures include data for several trailing-edge flap deflections for the two spanwise extents tested (η_F = 0.16 to 0.50 and η_F = 0.16 to 0.75). The data with suction are for flow conditions above the critical values and are representative for all of the porous extents listed in table IV.

Lift.- In figure 7, the trailing-edge-flap lift increments, ΔC_{L_F}, measured at 0.6° angle of attack are compared with the values predicted from the span loadings obtained by reference 10 and a theoretical $d\alpha/d\delta$ as suggested in reference 6.[1] The data shown in figure 7 indicate that this method can be used to estimate the lift increment obtained with an area-suction flap on the wing plan form tested. The poorest correlation was obtained with the 66° large span flap, and observation of the tufts showed that rough flow and separated flow existed aft of the porous area on the outer third of this large span flap. This flow was improved at 0° angle of attack, and the ΔC_{L_F}'s were increased (fig. 7(b)) by the addition of small fences on the flap at 0.33, 0.50, and 0.66 semispan stations. These fences had a height of about 5 percent of the chord, they extended from the aft edge of the porous area to the trailing edge, and they were located in a streamwise direction.

The ΔC_{L_F} of the 50° flap with the porous surfaces sealed are shown to be higher than those of the 61° or 66° flap with the porous surfaces sealed. Pressure distributions indicated that this resulted because partial attachment of the flow existed near the root of the 50° flap, but not with the 61° or 66° flap. Allowing air to circulate through the porous surface eliminated the partial attachment and reduced the flap lift increment of the 50° flap.

---

[1]The predicted

$$\Delta C_{L_F} = C_{L_{\delta_1}} \left(\frac{d\alpha}{d\delta}\right) \frac{\delta_{F_{streamwise}}}{57.3}$$

where $C_{L_{\delta_1}}$ for this wing was computed to be 1.26 and 1.93 for η_F = 0.16 to 0.50 and 0.16 to 0.75, respectively. A $(d\alpha/d\delta)$ = 0.565 for c_F/c = 0.217 was used and $\delta_{F_{streamwise}}$ was 48.8° for a 55° flap.

The flap lift increment with suction applied diminished with increasing angle of attack as shown in figure 8, but it also can be seen in this figure that the increment due to suction remained nearly constant.

Drag.- The measured increments of drag coefficient due to flap deflection at 0° angle of attack are presented in figure 9 as a function of the square of the flap lift coefficient at 0° angle of attack. Included in this figure are the curves of the theoretical drag-coefficient change with flap lift increment squared, computed using the span loadings obtained from reference 10 and the induced drag equations of reference 11.

Examination of the data in figure 9 shows that although the drag coefficient was increased at 0° angle of attack when suction was applied to the flap, the drag coefficient per unit flap lift coefficient squared was reduced. These data indicate that applying suction reduced the drag due to the separation of flow that existed on the flap without suction; however, this reduction in drag was of a smaller magnitude than the increase in the induced drag resulting from the increased flap lift increment produced by suction. It can also be seen that increasing the flap span reduced the drag coefficient per unit lift coefficient squared. Figure 9 also shows that the measured drag coefficient per unit flap lift increment with suction was greater than that computed and that the difference was greater with the smaller of the two flap spans.

The ratio of the experimental to theoretical drag-coefficient increment per increment of flap lift coefficient squared at 0° angle of attack, hereinafter referred to as the drag parameter, is presented in figure 10 in order to compare the data obtained for the present investigation with those of references 6 and 9. This figure indicates that application of suction to the flaps of all of the plan forms tested resulted in improved correlation with the theoretical induced drag calculations, implying that the drag due to separation of flow on the flap was greatly reduced by area suction. However, the only plan form for which good correlation was obtained with theory was the 45° swept-wing model of reference 9.

Pitching moment.- Applying area suction to the trailing-edge flaps resulted in more negative pitching-moment coefficients (fig. 6), this change being approximately proportional to the accompanying increase in lift coefficient. The measured increments of pitching-moment coefficient of the suction flaps are compared in figure 11 with the values predicted by the method of reference 12. This comparison indicates that good agreement existed between the measured and computed values of pitching moment.

Static longitudinal instability occurred at or near $C_{L_{max}}$ for all of the configurations for which data are presented in figure 6. Observation of tufts and surface pressures indicated that this instability was the result of the initial stall occurring from the leading edge of the wing near the wing tip, and that the stalled area moved inboard with increasing angle of attack.

[redacted]

Pressure distribution.- Chordwise surface pressure distributions for the 66° small-span flap (η_F = 0.16 to 0.50) with and without suction are given in figure 12 for four spanwise stations at several angles of attack. These pressure distributions are presented to show the change in pressure that occurs over the entire surface of the wing when suction is applied to a trailing-edge flap. This change in pressure is qualitatively the same for the other flap deflections and flap spans, but the magnitude of the change in pressure was dependent on the flap configuration.

Figures 12(d) and 12(e) also show that the leading-edge pressures at the wing tip collapsed suddenly when the angle of attack was increased near the angle for $C_{L_{max}}$. This collapse in pressure is an indication that air-flow separation occurred at the leading edge of the wing and limited the $C_{L_{max}}$ attainable.

The peak surface pressures measured for the different flap deflections at various spanwise stations are summarized in figure 13 and also compared with the values of peak pressure predicted from the results of reference 6. The reason for the large spanwise variation in peak pressure measured in the present test is not known. (It should be pointed out that the spanwise stations of the orifices in fig. 13 are referenced to the local hinge line and hence the orifices at 2y/b = 0.30 and 0.48 correspond to those of figure 12 at 2y/b = 0.35 and 0.53, respectively.)

The variation with angle of attack of the peak pressure coefficient at 2y/b = 0.30 on the trailing-edge flaps with area suction applied is presented in figure 14. It is seen that a reduction in peak negative pressure coefficient occurs with angle of attack for all of the suction flap configurations.

Integration of the distribution of surface pressures provided values of section lift coefficient. The variation of these section lift coefficients with angle of attack for the four spanwise stations is presented in figure 15 for the 66° deflection of the small-span flap (η_F = 0.16 to 0.50). Here again, the effect of suction can be seen in the increase in section lift at each of the spanwise stations.

Suction requirements.- The variation of $C_{Q_{F_{crit}}}$ with chordwise extent and location of porous area is shown in figure 16 for various deflections of the small-span flap with the constant porosity material. In figure 17, the variation of the minimum $C_{Q_{F_{crit}}}$ with flap deflection is presented and compared with values predicted by the method of reference 6. (The reference areas for the 44° wing are 0.37 and 0.56 for η_F = 0.16 to 0.50 and 0.16 to 0.75, respectively.) The data of this figure show good correlation with the values predicted. Further, it is seen that using a porous material with a porosity variation in the chordwise direction compensating for the variation in surface pressures resulted

in a reduction in the $C_{Q_{F_{crit}}}$. This reduction in $C_{Q_{F_{crit}}}$ was of the same magnitude as predicted in reference 6. The duct pressure coefficient required at 0.6° angle of attack for $C_{Q_{F_{crit}}}$ with the optimum opening is compared in figure 18 with the maximum peak negative surface pressure coefficient on the flap. It can be seen that the duct pressure coefficient is primarily determined by the peak surface pressure on the trailing-edge flap. The following table summarizes the suction requirements of the trailing-edge flaps at two angles of attack for two free-stream velocities:

α, deg	δ_F, deg	2y/b	Configuration	U = 156 ft/sec			U = 202 ft/sec		
				ΔC_{L_F}	$C_{Q_{F_{crit}}}$	$P_{d_{F_{crit}}}$	ΔC_{L_F}	$C_{Q_{F_{crit}}}$	$P_{d_{F_{crit}}}$
0.5	50	0.16-0.50	3	0.61	0.00032	-4.6	0.62	0.00036	-4.7
10.9				.56	.00038	-3.8	.55	.00037	-3.8
.5	61		9	.68	.00046	-5.3	.69	.00046	-5.3
10.9				.60	.00055	-4.5	.60	.00057	-4.4
.6	66		19	.71	.00070	-5.3	.71	.00072	---
11.0				.63	.00070	-4.6	---	---	---
.7	50	0.16-0.75	23	.87	.00061	-5.2	---	---	---
6.9				.80	.00075	-4.9	---	---	---
.8	66		29	1.00	.00128	-5.5	---	---	---
9.1				.89	.00141	-4.8	---	---	---

It can be seen that the effects of angle of attack and of free-stream velocity on the $C_{Q_{F_{crit}}}$ were small. The duct pressure coefficient is primarily determined by the peak surface pressure coefficient; therefore, the variation of the P_{d_F} with angle of attack was similar to that of the peak surface pressure coefficient presented in figure 14.

Effect of boundary-layer thickness on suction requirements.- Limited tests were also made with a thickened boundary layer forward of the 61° small-span flap to see if the suction requirements would be altered. The results of these tests are presented in figure 19 where the ΔC_{L_F} variation with C_{Q_F} for the 61° flap having a normal boundary layer is compared with those of the flap having a thicker wing boundary layer and also for the flap having a thicker fuselage boundary layer. The wing boundary layer, measured 9 inches forward of the porous area and 11 inches outboard of the fuselage, was increased from 1.6 to 2.0 inches by a spoiler on the forward portion of the wing. The fuselage boundary layer, measured 2.5 inches above the wing and 7 inches forward of the porous area, was increased from 1.6 to 4.0 inches by a spoiler on the fuselage. Comparison

of the data of figure 19 indicate that increasing the boundary-layer thicknesses to the values mentioned previously had no measurable effect on the suction flow or pressure requirements.

In a previous investigation, it was found that locating the inboard edge of the porous surface within the fuselage boundary layer reduced the flap lift increments (see ref. 7). In the present test the 61° small-span flap was also extended to the fuselage, and contrary to the detrimental results obtained in reference 7, a slight increase in ΔC_{L_F} was measured (an increase in ΔC_{L_F} of about 0.01). Increasing the fuselage boundary-layer thickness from 1.6 to 4.0 inches did not affect either the lift increment or suction requirements.

Model With Undeflected Leading-Edge Flap and With a Horizontal Tail

The longitudinal characteristics of the model with a horizontal tail are presented in figure 20. These characteristics were measured with an undeflected flap, 66° short-span flap with suction, and 66° long-span flap with suction. Comparison of the data of figure 20 with those of figure 6 indicates that the addition of the horizontal tail to the configuration with flaps deflected did not eliminate the instability that existed near $C_{L_{max}}$ for the model with the horizontal tail off.

Model With Leading-Edge Flap Deflected and Without a Horizontal Tail

Lift, drag, and pitching moment.- The data in figure 21 are presented to show how the characteristics of the wing were affected when the nose flap was deflected 40° and area suction was applied to it. Data in figure 21(a) are for the trailing-edge flap undeflected, data in figure 21(b) are for the small-span flap deflected 66° with and without suction applied, and the data in figure 21(c) are for the large-span flap deflected 66° with and without suction. The data shown with suction applied are for conditions of suction flow at or above the critical values.

The use of a nose flap with and without area suction delayed leading-edge air-flow separation for all of the trailing-edge-flap configurations. The values of $C_{L_{max}}$ measured for various configurations are summarized in the following table:

δ_N	$C_{L_{max}}$ for $\delta_F = 0^\circ$	$C_{L_{max}}$ for $\delta_F = 66^\circ$, $\eta_F = 0.16$ to 0.50 with suction	$C_{L_{max}}$ for $\delta_F = 66^\circ$, $\eta_F = 0.16$ to 0.75 with suction
0	1.08	1.34	1.48
40° sealed	1.30	1.48	1.62
40° suction	1.68	2.00	2.00

The variations of ΔC_{l_F} with angle of attack are presented in figure 22 for the model with the nose flap deflected 40° and suction applied to it. These data show that when leading-edge separation is delayed the flap lift increments are maintained to high angles of attack. However, the ΔC_{l_F}, with suction, decreased with increased angle of attack, and the increase in $C_{L_{max}}$ due to applying suction to the trailing-edge flap was small (figs. 21(b) and 21(c)). The data for the small-span flap presented in figure 21(b) show that an increase in lift-curve slope occurred at 13° angle of attack for the 66° flap without suction. Observations of the pressures indicated that partial attachment of the flow on the inboard section of the flap occurred at these angles of attack. Re-examination of the data for the same trailing-edge flap with the leading-edge flap undeflected (fig. 6(a)) also shows this increase in lift-curve slope at about the same angle of attack.

Since the suction nose flap delayed the air-flow separation on the wing to higher lift coefficients, the abrupt rise in drag coefficient and the abrupt change in pitching moment were also delayed by the use of the suction nose flap (fig. 21). It may be noted in figure 21(c) that there was a gradual decrease in the stability with the large-span trailing-edge flap as the angle of attack was increased. The surface pressure distributions indicated that this decrease in stability was primarily due to increased separation that occurred on the outboard portion of the trailing-edge flap as the angle of attack was increased.

Pressure distribution.- Chordwise pressure distributions at four spanwise stations for several angles of attack are given in figure 23 for the model with the nose flap deflected with and without suction applied. These data are presented for the small-span trailing-edge flap deflected 66° and with suction applied. These figures show graphically the effect of applying area suction to the leading-edge flap. The effect on the pressure distribution when suction was applied to the nose flap was similar for the other trailing-edge flap configurations tested. Integration of the pressure distribution of figure 23 provided the section lift coefficient variation with angle of attack presented in figure 24. The nonlinear variation of the section lift of the flapped stations with angle of attack results from the decrease in ΔC_{l_F} with increasing angle of attack that was previously noted.

Suction requirements.- The effect of the chordwise extent of porous area on the critical flow coefficient for the nose flap, $C_{Q_{N_{crit}}}$, is shown in figure 25 for the model with the trailing-edge flap undeflected. This figure includes values of $C_{Q_{N_{crit}}}$ for the constant porosity material as well as for porous material with a variation in porosity compensating for the variation in surface pressures. It should be noted that the forward edge of the openings tested (1/2 inch ahead of the midarc of the flap) was very close to the location of the peak pressure on the nose flap. This figure shows that the use of the tapered porous felts greatly reduced the critical suction flow coefficients.

The variation of $C_{Q_{N_{crit}}}$ with lift coefficient for the nose flap with a variable porosity material is shown in figure 26 for the model with an undeflected trailing-edge flap and for the 66° small- and large-span flaps.

The variation with lift coefficient of the duct pressure coefficient required for the nose flap at $C_{Q_{N_{crit}}}$ is shown in figure 27 for the model with an undeflected trailing-edge flap and with the 66° small- and large-span flaps.

A limited amount of data was taken to determine the suction requirements of the trailing-edge flap at angles of attack above those attainable without air-flow separation with the nose flap undeflected. The results of these measurements are summarized in table VI for the 66° deflection with both flap spans. The primary effect of increased angle of attack on the suction requirements was the reduction in the duct pressure coefficient which resulted from the reduced external pressure over the knee of the trailing-edge flap; similar results were noted previously for a lower angle-of-attack range for the model with the undeflected nose flap.

Model With Leading-Edge Flap Deflected and With a Horizontal Tail

Figure 28 presents a comparison of the three-component force data measured with the horizontal tail on and off the model having a 40° leading-edge flap with suction and the 66° trailing-edge flap (η_F = 0.16 to 0.75) with suction. These data show that the use of the horizontal tail increased the stability of the model throughout the angle-of-attack range.

CONCLUDING REMARKS

The first portion of the wind-tunnel investigation of a 44° swept-wing model having trailing-edge area-suction flaps was conducted with an undeflected leading-edge flap. The results of these tests indicated that applying area suction at the knee of the trailing-edge flap increased the lift provided by the flap up to the maximum lift coefficient of the model. It was also found that the suction requirements and the changes in force characteristics at 0° angle of attack for the suction trailing-edge flap could be predicted by methods set forth in previous reports.

The second portion of the investigation was made to determine the effectiveness of a leading-edge area-suction flap in delaying the air-flow separation from the leading edge of the 44° swept-wing model. It was found that using a 40° leading-edge flap with area suction at the knee increased the maximum lift coefficient from 1.4 to 2.0 for the model with the trailing-edge area-suction flap deflected.

Ames Aeronautical Laboratory
National Advisory Committee for Aeronautics
Moffett Field, Calif., June 1, 1956

REFERENCES

1. Cook, Woodrow L., and Kelly, Mark W.: The Use of Area Suction for the Purpose of Delaying Separation of Air Flow at the Leading Edge of a 63° Swept-Back Wing - Effects of Controlling the Chordwise Distribution of Suction-Air Velocities. NACA RM A51J24, 1952.

2. Holzhauser, Curt A., and Martin, Robert K.: The Use of Leading-Edge Area Suction to Increase the Maximum Lift Coefficient of a 35° Swept-Back Wing. NACA RM A52G17, 1952.

3. Bray, Richard S., and Innis, Robert C.: Flight Tests of Leading-Edge Area Suction on a Fighter-Type Airplane With a 35° Sweptback Wing. NACA RM A55C07, 1955.

4. Holzhauser, Curt A., and Martin, Robert K.: The Use of a Leading-Edge Area-Suction Flap to Delay Separation of Air Flow From the Leading Edge of a 35° Sweptback Wing. NACA RM A53J26, 1953.

5. Poppleton, E. D.: Boundary-layer Control for High Lift by Suction at the Leading-edge of a 40 deg Swept-back Wing. R. & M. No. 2897, British A.R.C., 1955.

6. Cook, Woodrow L., Holzhauser, Curt A., and Kelly, Mark W.: The Use of Area Suction for the Purpose of Improving Trailing-Edge Flap Effectiveness on a 35° Sweptback Wing. NACA RM A53E06, 1953.

7. Kelly, Mark W., and Tolhurst, William H., Jr.: The Use of Area Suction to Increase the Effectiveness of a Trailing-Edge Flap on a Triangular Wing of Aspect Ratio 2. NACA RM A54A25, 1954.

8. Anderson, Seth B., and Quigley, Hervey C.: Flight Measurements of the Low-Speed Characteristics of a 35° Swept-Wing Airplane With Area-Suction Boundary-Layer Control on the Flaps. NACA RM A55K29, 1956.

9. Griffin, Roy N., Jr., and Hickey, David H.: Investigation of the Use of Area Suction to Increase the Effectiveness of Trailing-Edge Flaps of Various Spans on a Wing of 45° Sweepback and Aspect Ratio 6. NACA RM A56B27, 1956.

10. DeYoung, John: Theoretical Symmetric Span Loading Due to Flap Deflection for Wings of Arbitrary Plan Form at Subsonic Speeds. NACA Rep. 1071, 1952.

11. DeYoung, John, and Harper, Charles W.: Theoretical Span Loading at Subsonic Speeds for Wings Having Arbitrary Plan Form. NACA Rep. 921, 1950.

12. James, Harry A., and Hunton, Lynn W.: Estimation of Incremental Pitching Moments Due to Trailing-Edge Flaps on Swept and Triangular Wings. NACA RM A55D07, 1955.

TABLE I.- COORDINATES OF THE AIRFOIL SECTION IN THE PLANE NORMAL TO THE 0.25-CHORD STATION

Airfoil station 1		Airfoil station 2	
Percent chord	Upper and lower ordinates, percent chord	Percent chord	Upper and lower ordinates, percent chord
0	0	0	0
.42	.95	.56	1.10
.63	1.17	.82	1.32
1.05	1.49	1.35	1.66
2.16	2.03	2.69	2.25
4.3	2.72	5.36	2.98
6.5	3.19	8.0	3.47
8.6	3.54	10.7	3.85
12.95	4.07	16.0	4.41
17.3	4.43	21.3	4.82
21.6	4.70	26.7	5.09
26.0	4.88	32.0	5.29
30.3	4.98	37.3	5.40
34.7	5.03	42.7	5.44
39.0	4.99	48.0	5.40
43.4	4.88	53.3	5.28
47.8	4.70	58.6	5.08
52.1	4.45	64.0	4.80
56.4	4.14	69.3	4.46
60.8	3.76	75.0[a]	3.62
65.2	3.30		
73.8[a]	1.91		
100.0[b,c]	0	100.0[b,c]	0
87.0[d]		106.50[d]	
Leading-edge radius 1.33		Leading-edge radius 1.32	

[a]Hinge line of trailing-edge flap.
[b]Trailing-edge of wing.
[c]Sections are straight lines from the hinge line to the trailing edge.
[d]Trailing-edge of wing of reference 4.

TABLE II.- LOCATION OF SURFACE PRESSURE ORIFICES

(a) Leading-edge flap undeflected; trailing-edge flap deflected 66° from 2y/b = 0.16 to 0.50

[Percent chord in plane 10° from plane of symmetry (see fig. 2)]

η = 0.35		η = 0.53		η = 0.71		η = 0.89	
Upper	Lower	Upper	Lower	Upper	Lower	Upper	Lower
0	0.23	0	0.24	0	0.25	0	0.26
.23	.46	.24	.48	.25	.98	.26	1.04
.46	.92	.48	.95	.98	1.97	.52	2.08
.92	1.39	.95	1.43	1.38	9.84	1.04	3.63
1.39	1.85	1.43	1.91	1.97	19.69	1.56	5.19
1.85	2.31	1.91	2.38	2.46	39.35	2.08	10.37
2.31	4.62	2.38	4.76	6.15	59.01	2.59	20.74
4.62	6.94	3.34	7.14	7.38	85.00	3.63	41.50
5.78	9.24	4.76	9.52	9.84	89.07	5.19	62.20
6.94	13.87	5.95	14.26	14.76		6.48	83.00
9.24	27.73	7.14	28.53	19.69		7.78	97.50
13.87	37.00	9.52	38.05	39.37		10.37	
27.73	69.35	14.26	57.07	59.05		15.56	
37.00	74.00	28.53	66.60	73.80		20.74	
46.25	78.42	38.05	71.35	85.00		31.10	
55.50	80.37	47.57	76.10	97.50		41.50	
64.75	82.93	57.07	81.14			62.20	
69.35	86.64	66.60	83.46			72.60	
74.00		71.35	67.46			83.00	
78.42		76.10				90.00	
78.86		78.98				97.50	
79.29		79.52					
79.68		79.98					
80.04		80.40					
80.41		80.78					
81.81		81.33					
83.02		82.82					
84.79		83.83					
87.13		85.31					
		87.82					

TABLE II.- LOCATION OF SURFACE PRESSURE ORIFICES - Concluded
(b) Leading-edge flap deflected 40°; trailing-edge flap deflected 66° from 2y/b = 0.16 to 0.50
[Percent chord in plane 10° from plane of symmetry (see fig. 2)]

η = 0.35		η = 0.53		η = 0.71		η = 0.89	
Upper	Lower	Upper	Lower	Upper	Lower	Upper	Lower
0	1.08	0	1.11	0	1.15	0	1.21
0	1.48	0	1.52	0	2.28	0	2.41
0	2.15	0	2.21	.19	3.49	0	3.68
.17	2.75	.18	2.83	.36	11.51	.20	12.14
.34	3.29	.35	3.38	.60	19.18	.38	20.74
.58	4.81	.60	4.95	.89	39.35	.65	41.50
.83	6.29	.86	6.47	3.29	59.01	.93	62.20
2.28	8.62	2.35	8.86	4.18	82.71	1.53	97.50
3.10	10.82	3.19	11.14	5.96	89.07	4.41	
3.93	13.87	4.04	14.26	6.37		6.28	
5.50	27.73	5.76	28.53	7.16		6.71	
5.86	37.00	6.14	38.05	8.00		6.98	
6.59	69.35	6.90	50.07	8.94		8.93	
7.29	74.00	7.72	66.60	9.69		9.42	
8.03	80.37	8.58	71.35	10.92		10.20	
8.92	82.93	9.48	76.10	11.94		11.51	
9.76	86.64	10.36	81.14	12.96		12.59	
10.66		11.33	83.46	14.76		13.66	
11.56		12.30	87.46	19.69		15.56	
13.87		14.26		39.37		20.74	
27.73		28.53		59.05		31.10	
37.00		38.05		85.00		41.50	
46.25		47.57		97.50		62.20	
55.50		57.07				72.60	
64.75		66.60				83.00	
69.35		71.35				90.00	
74.00		76.10				97.50	
78.42		78.98					
78.86		79.52					
79.29		79.98					
79.68		80.40					
80.04		80.78					
80.41		81.33					
81.81		82.82					
83.02		83.83					
84.79		85.31					
87.13		87.82					

TABLE III.- COORDINATES OF THE FUSELAGE

Fuselage station, in.	Radius, in.
0	0
2	2.5
4	3.8
6	4.8
12	7.3
18	9.4
24	11.1
30	13.1
36	14.6
42	15.9
48	17.0
54	18.0
60	18.9
72	20.6
84	21.9
96	23.9
102	23.6
114	24.6
132	25.7
150	27.0
168	28.3
186	29.0
204	29.6
330	29.6
346	29.1
362	27.9
381	25.8
400	23.7
419	21.6
438	19.5
450	18.2
468	16.2
486	14.2
510	11.6

TABLE IV.- POROUS AREA CONFIGURATIONS TESTED
[Porous material constant porosity unless otherwise noted]

(a) Trailing-edge flap			
Configuration	δ_F, deg	Spanwise extent, 2y/b	Porous opening, in. (referenced to midarc of flap, see fig. 2(c))
1	0		
2	50	0.16 to 0.50	sealed
3	↓	↓	0 to 1-1/2
4			0 to 2-1/2
5			0 to 4-1/4
6	↓		0 to 6
7	61		sealed
8	↓		-1/2 to 1
9			-1/2 to 2
10			-1/2 to 2[a]
11			-1/2 to 3
12			-1/2 to 4-3/4
13			-1/2 to 6-1/2
14			1/2 to 3
15	↓		-1-1/2 to 1
16	66		sealed
17	↓		-1/2 to 1
18			-1/2 to 2
19			-1/2 to 3
20			-1/2 to 4-3/4
21	↓	↓	-1/2 to 6-1/2
22	50	0.16 to 0.75	sealed
23	↓	↓	0 to 1-1/2
24			0 to 1-1/2[b]
25			0 to 2-1/2
26	↓		0 to 1-1/2 at root 0 to 2-1/2 at tip
27	66		sealed
28	↓		-1/2 to 2
29			-1/2 to 3
30			-1/2 to 3[b]
31	↓		-1/2 to 1 at root -1/2 to 2 at tip
32	↓	↓	-1/2 to 1-1/2 at root -1/2 to 4-1/2 at tip

(b) Leading-edge flap deflected 40°		
Configuration	Porous opening, in.	Porous material
33	sealed	
34	-1/2 to 1-1/2	constant porosity
35	-1/2 to 1-1/2	variable porosity
36	-1/2 to 2	constant porosity
37	-1/2 to 2	variable porosity
38	-1/2 to 2-1/2	constant porosity

[a]Variable porosity.
[b]Three fences on flap at 2y/b = 0.33, 0.50, and 0.62.

TABLE V.- MODEL CONFIGURATIONS TESTED

Figure	Leading-edge flap		Trailing-edge flap		Horizontal tail	Free-stream velocity, ft/sec
	δ_N, deg	Configuration (table IV)	δ_F, deg	Configuration (table IV)		
6(a)	0		0,50,61,66	1,2,3,7,9,16,19	off	156
6(b)	0		0,50,66	22,23,27,29	off	156
12,15	0		66	16,19	off	156
16	0		50,61,66	3-6,8,9,11-15,17-21	off	156
17	0		50,61,66	3,9,10,19,23,24,29,30	off	156
19	0		61	9	off	156
20	0		0,66	1,19,29	on	156
21(a)	40	33,37	0	1	off	156
21(b),22,23	40	33,37	66	19	off	156
21(b)	40	37	66	16	off	156
21(c)	40	33,37	66	29	off	156
21(c)	40	37	66	27	off	156
25	40	34-38	0	1	off	156
26,27	40	37	0,66	1,19,29	off	156
28	40	37	66	29	on	156
(1)	0		50,66	24,25,26,28,30,31,32	off	156
	0		50,61,66	3,9,10,19	off	202

[1]Configurations for which data are not presented.

TABLE VI.- SUCTION REQUIREMENTS OF THE TRAILING-EDGE FLAPS WITH THE 40° LEADING-EDGE FLAP (CONFIGURATION 37 WITH SUCTION); HORIZONTAL TAIL OFF, U = 156 FEET PER SECOND

(a) $\delta_F = 66^\circ$, $\eta_F = 0.16$ to 0.50, configuration 19				(b) $\delta_F = 66^\circ$, $\eta_F = 0.16$ to 0.75, configuration 29			
α	ΔC_{L_F}	$C_{Q_F crit}$	$P_{d_F crit}$	α	ΔC_{L_F}	$C_{Q_F crit}$	$P_{d_F crit}$
0.6	0.73	0.00067	-5.4	0.8	1.01	0.00126	-5.6
11.0	.64	.00063	-4.7	11.1	.88	.00138	-4.5
21.3	.51	.00053	-3.3	21.5	.67	.00140	-3.2

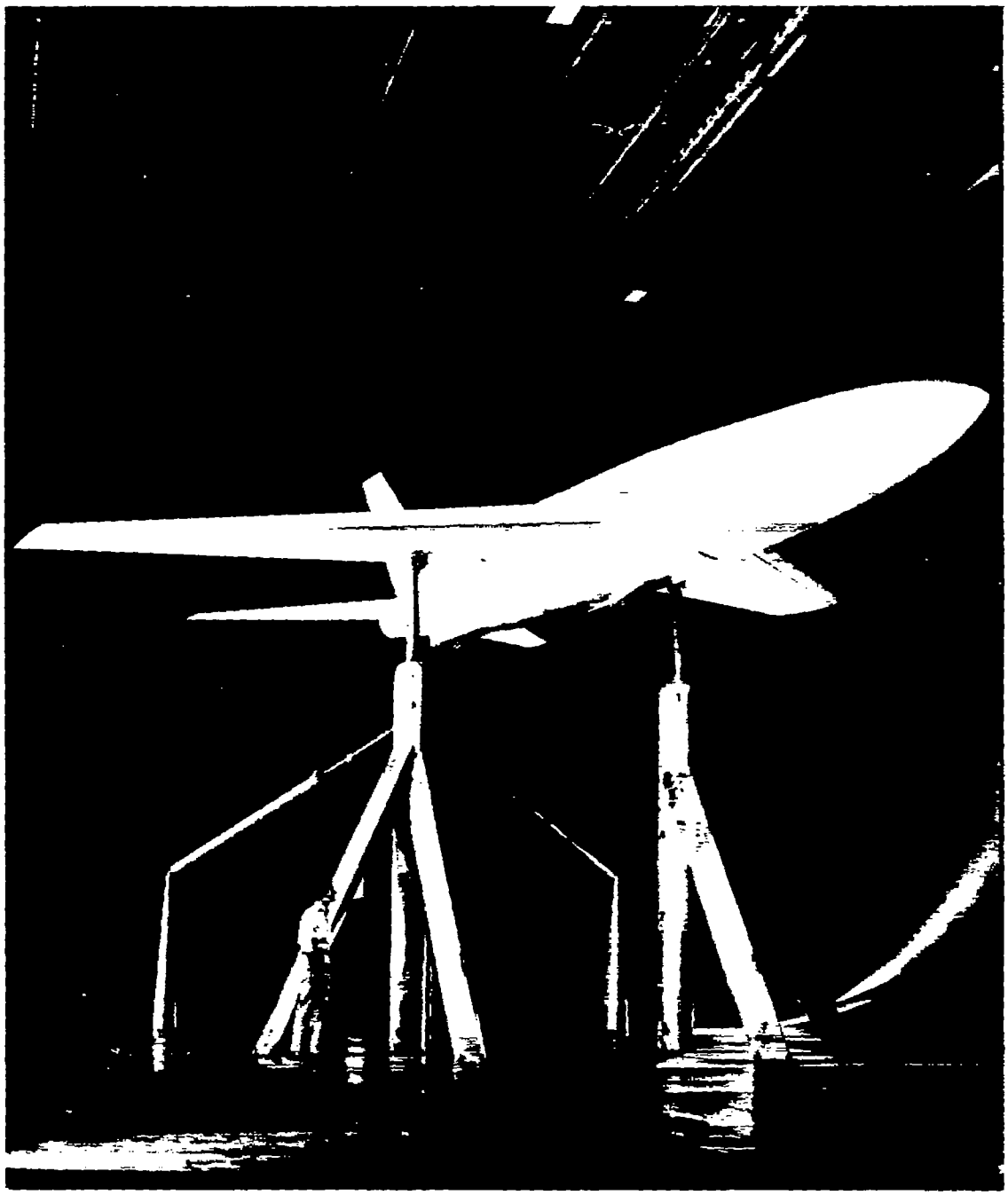

A-19443

(a) Flaps undeflected.

Figure 1.- Model in the 40- by 80-foot wind tunnel.

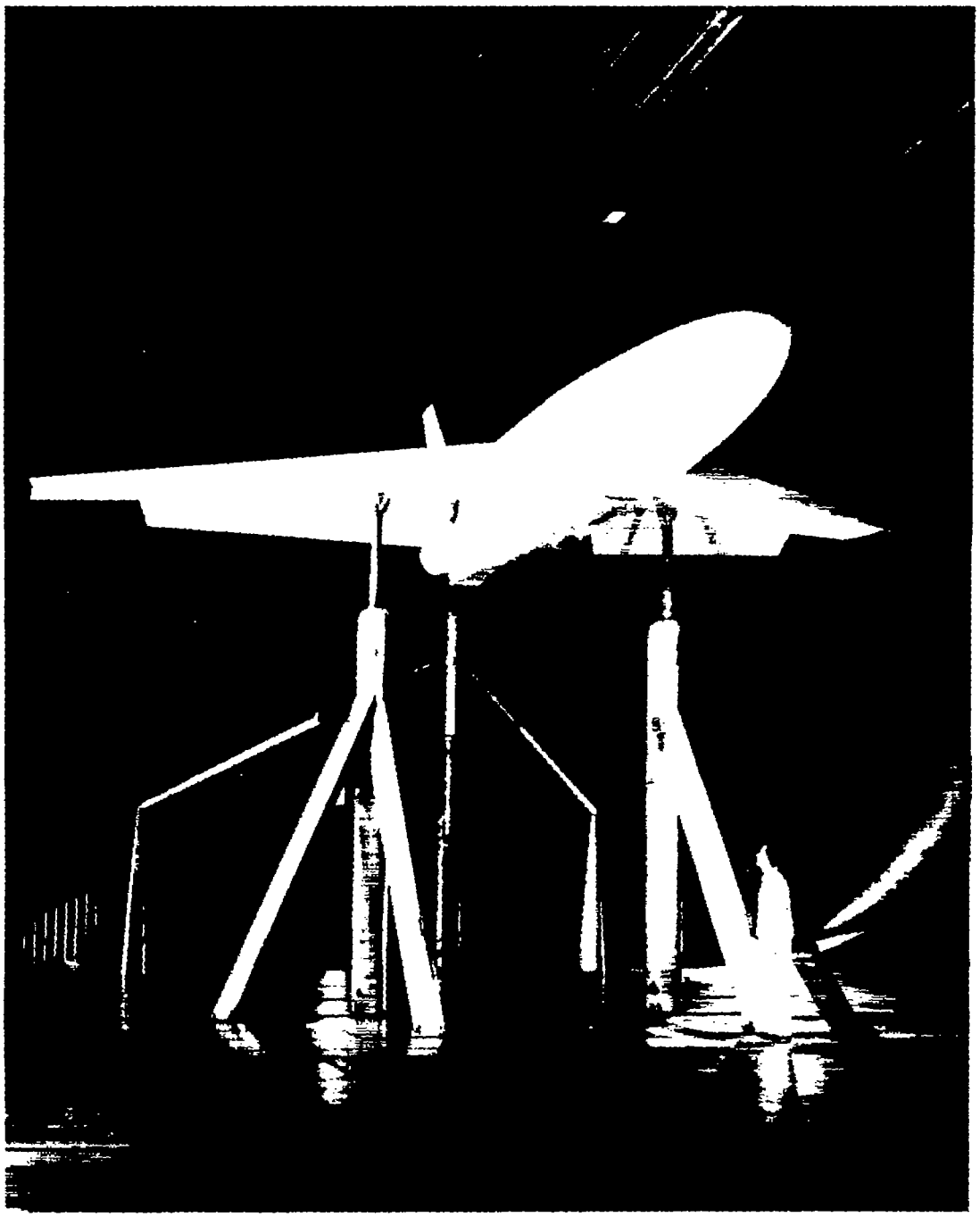

A-19438

(b) Leading-edge flap and large-span trailing-edge flap deflected.

Figure 1.- Concluded.

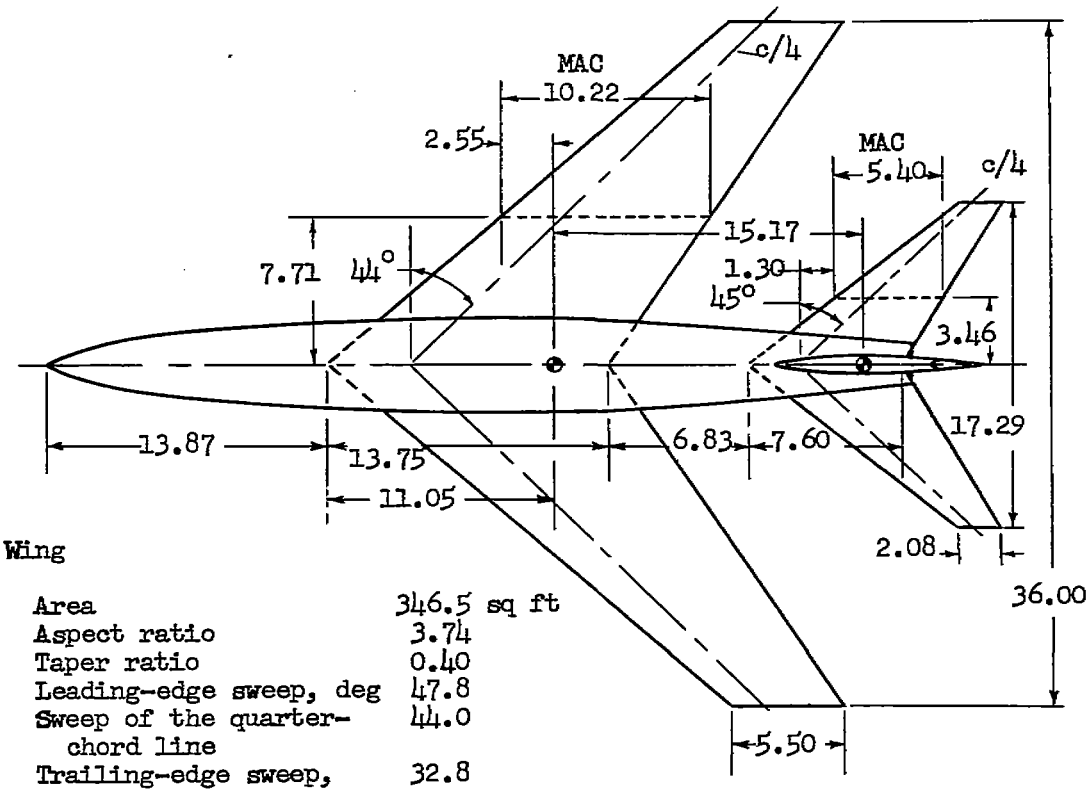

Wing

Area	346.5 sq ft
Aspect ratio	3.74
Taper ratio	0.40
Leading-edge sweep, deg	47.8
Sweep of the quarter-chord line	44.0
Trailing-edge sweep, deg	32.8

Horizontal Tail

Area	83.8 sq ft
Aspect ratio	3.27
Taper ratio	0.27

Vertical Tail

Area	35.0 sq ft
Aspect ratio	1.87
Taper ratio	0.40

All dimensions in feet and degrees unless otherwise noted.

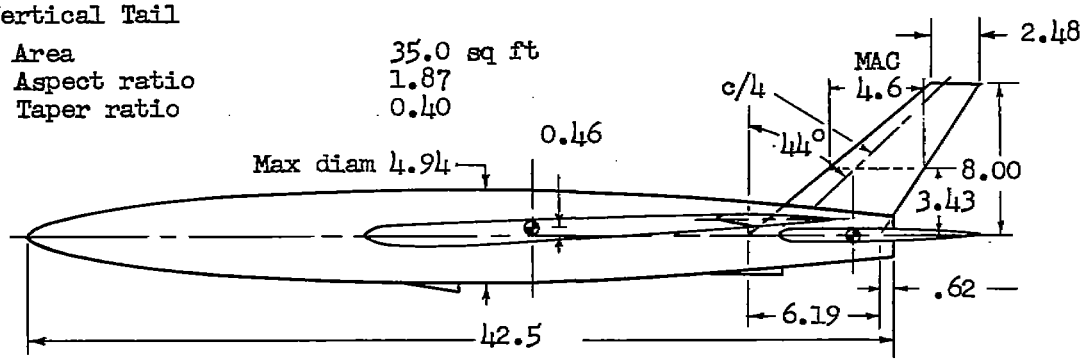

(a) Complete model.

Figure 2.- Geometry of 44° sweptback-wing model.

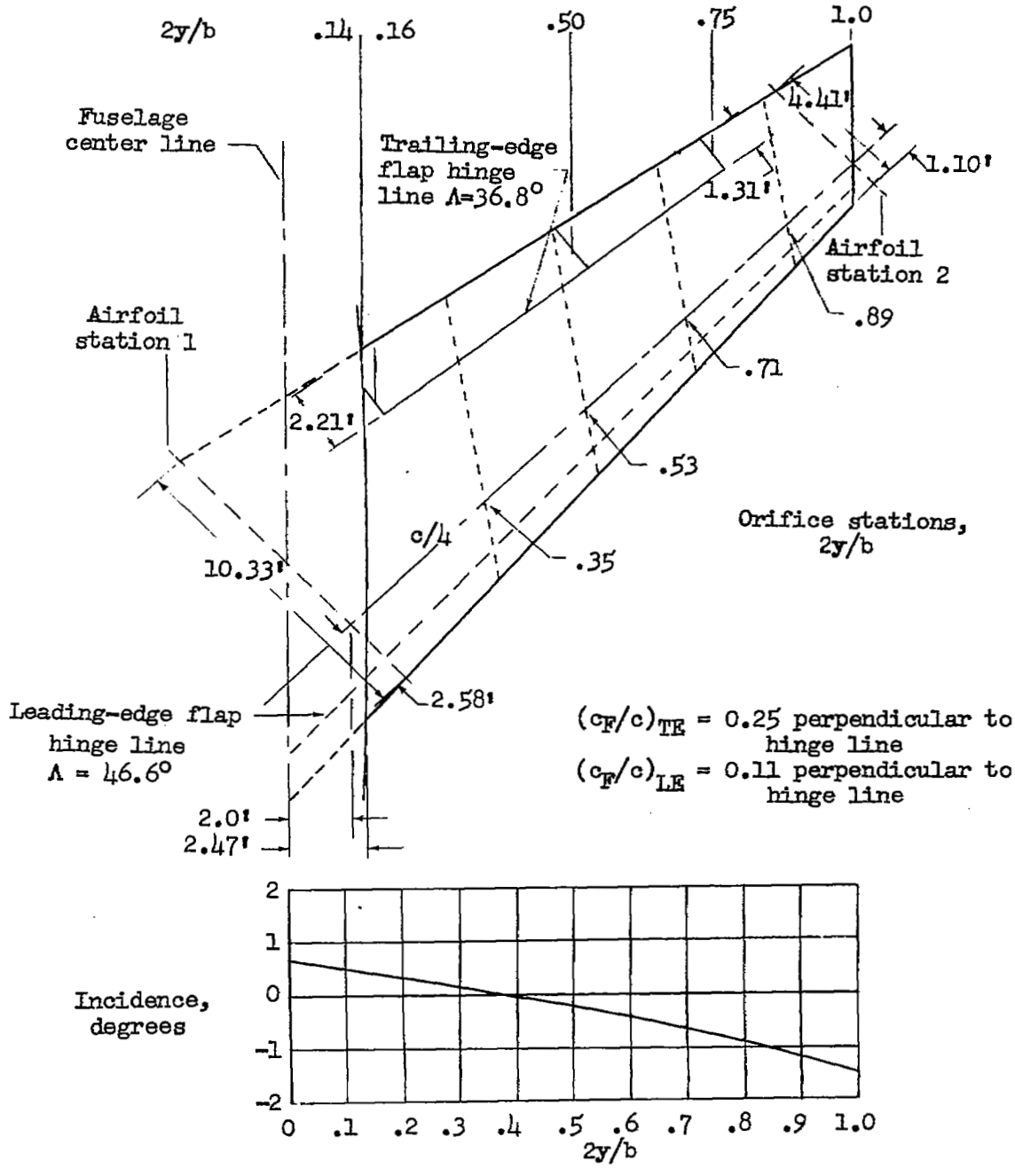

(b) Details of the wing.

Figure 2.- Continued.

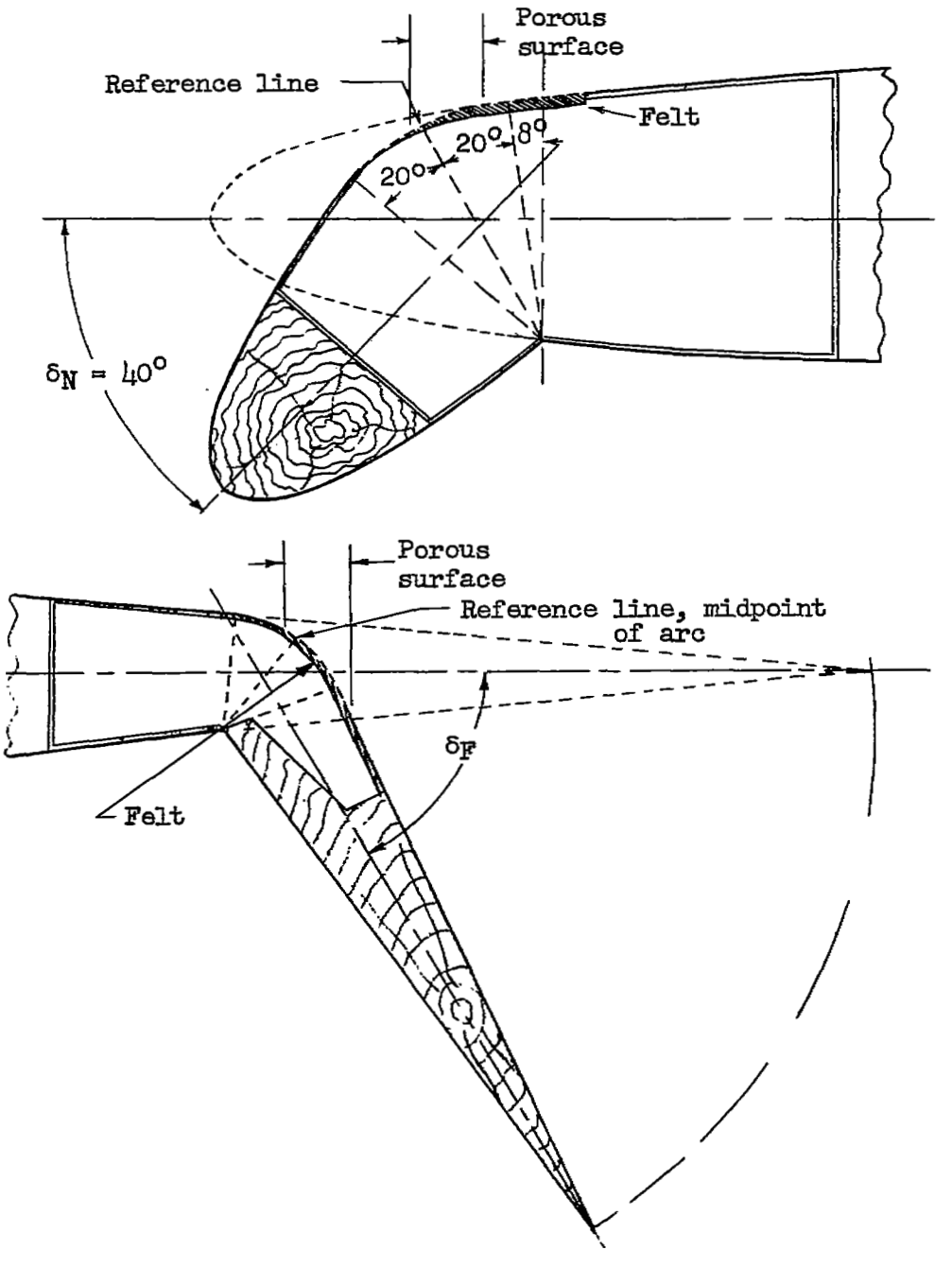

(c) Cross section of deflected leading-edge and trailing-edge flap.

Figure 2.- Concluded.

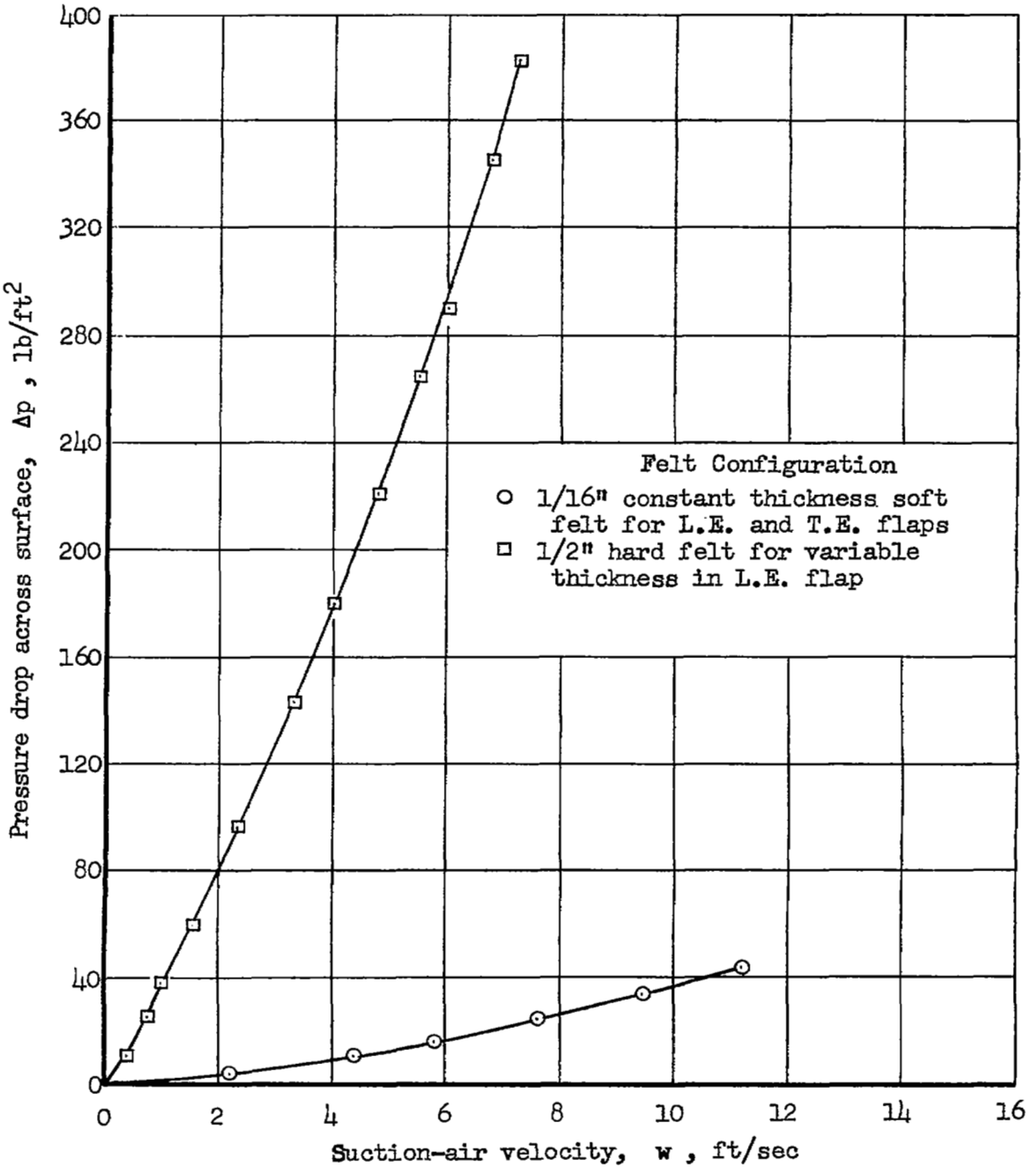

Figure 3.- Calibration of suction-air velocities for the metal mesh screen backed with wool felt material.

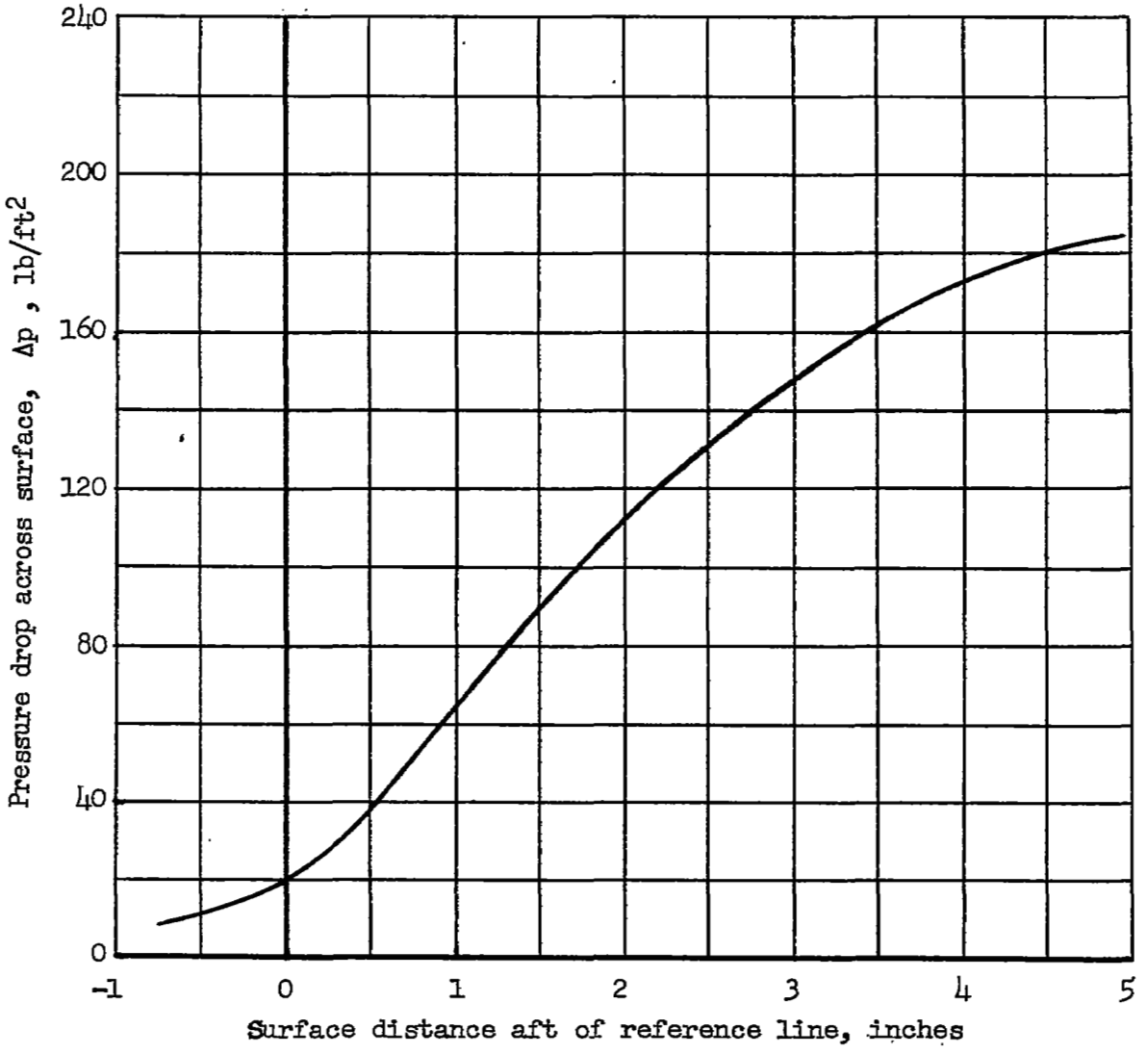

Figure 4.- Variation of pressure drop across porous stainless steel with surface distance for an average inflow velocity of 3.75 feet per second; thickness of steel equal to 0.05 inch.

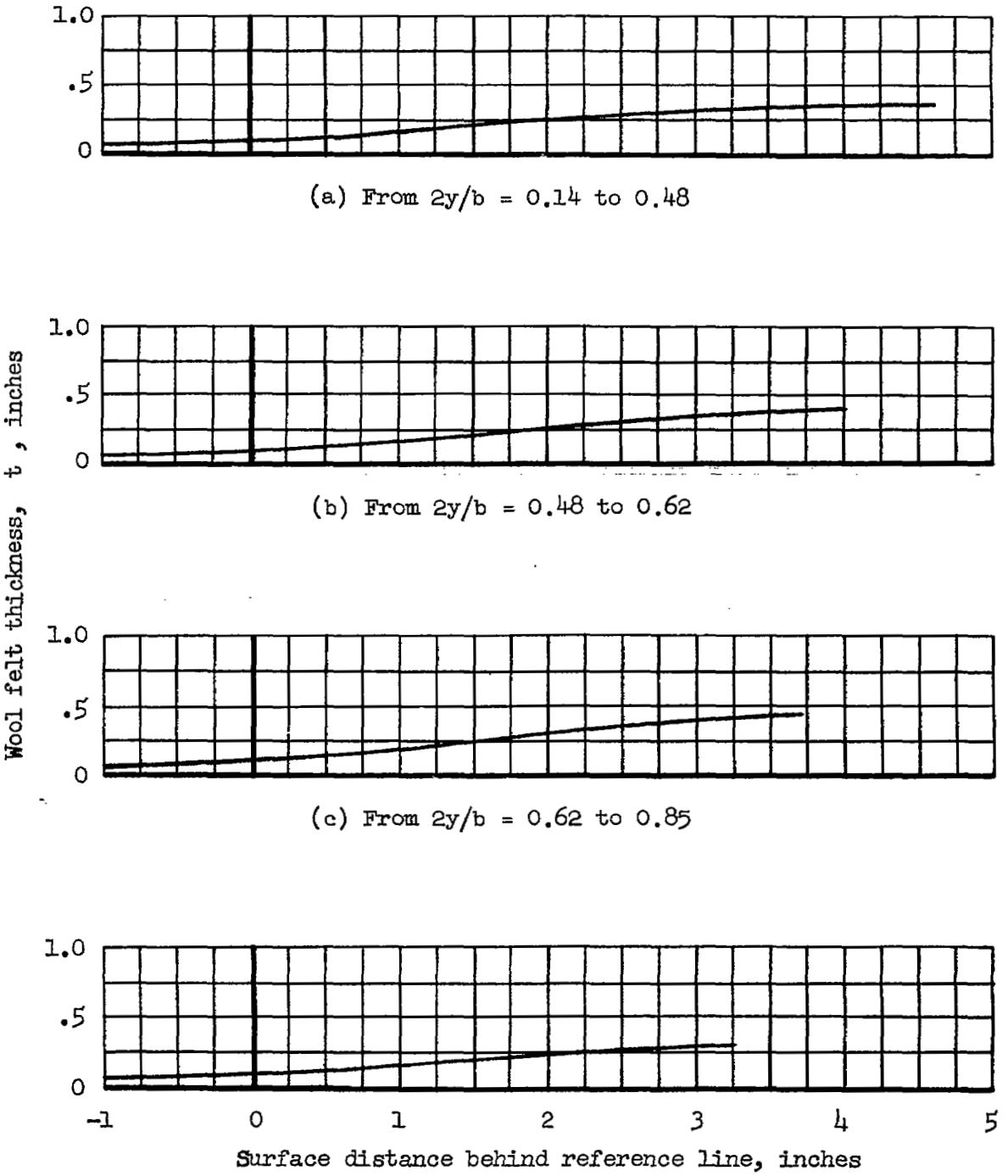

Figure 5.- Thickness variations of the felt backing used in the leading-edge flap.

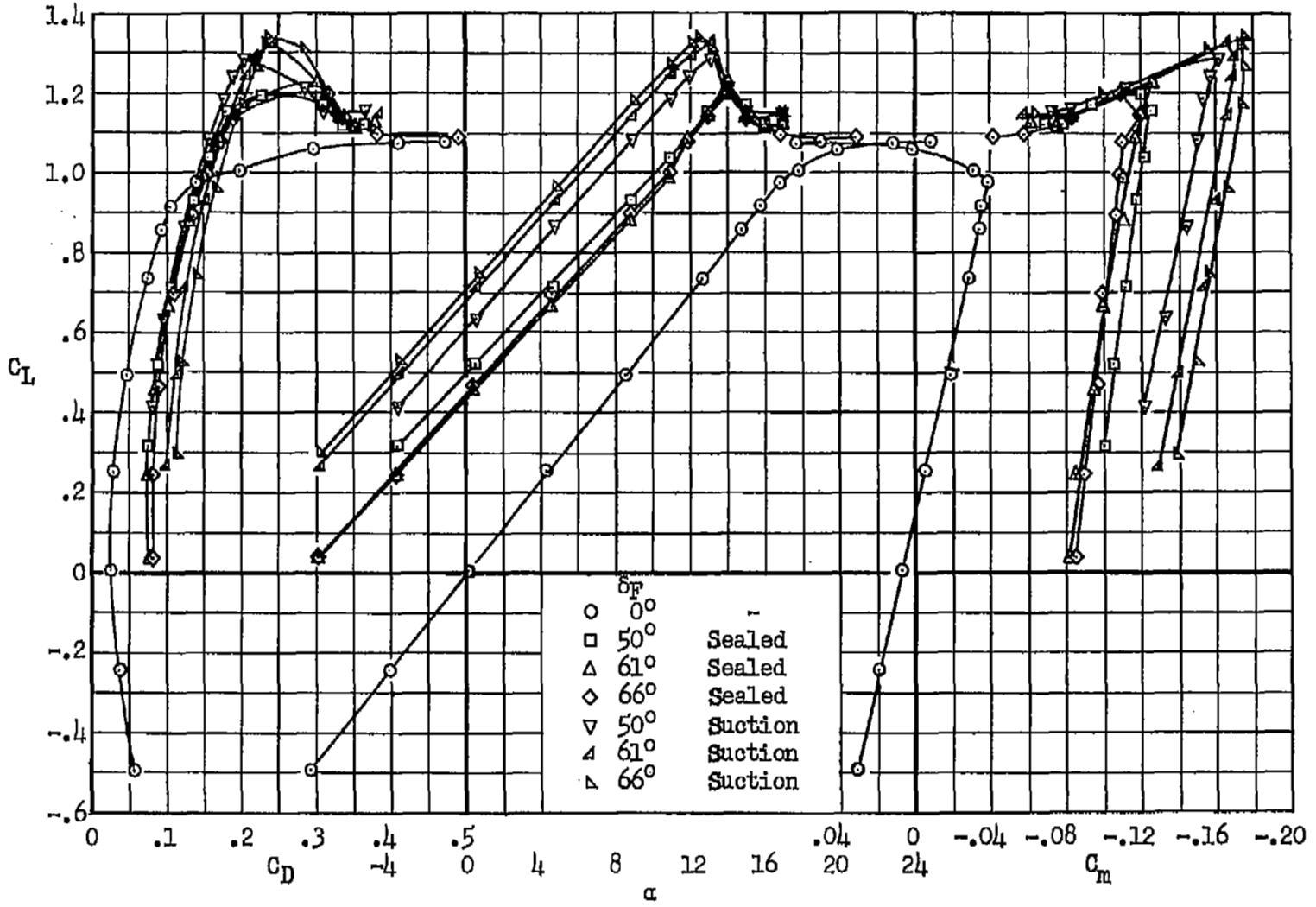

(a) Flap span; η_F = 0.16 to 0.50.

Figure 6. Longitudinal characteristics of the model with various trailing-edge flap configurations; $\delta_N = 0^\circ$, horizontal tail off, U = 156 ft/sec.

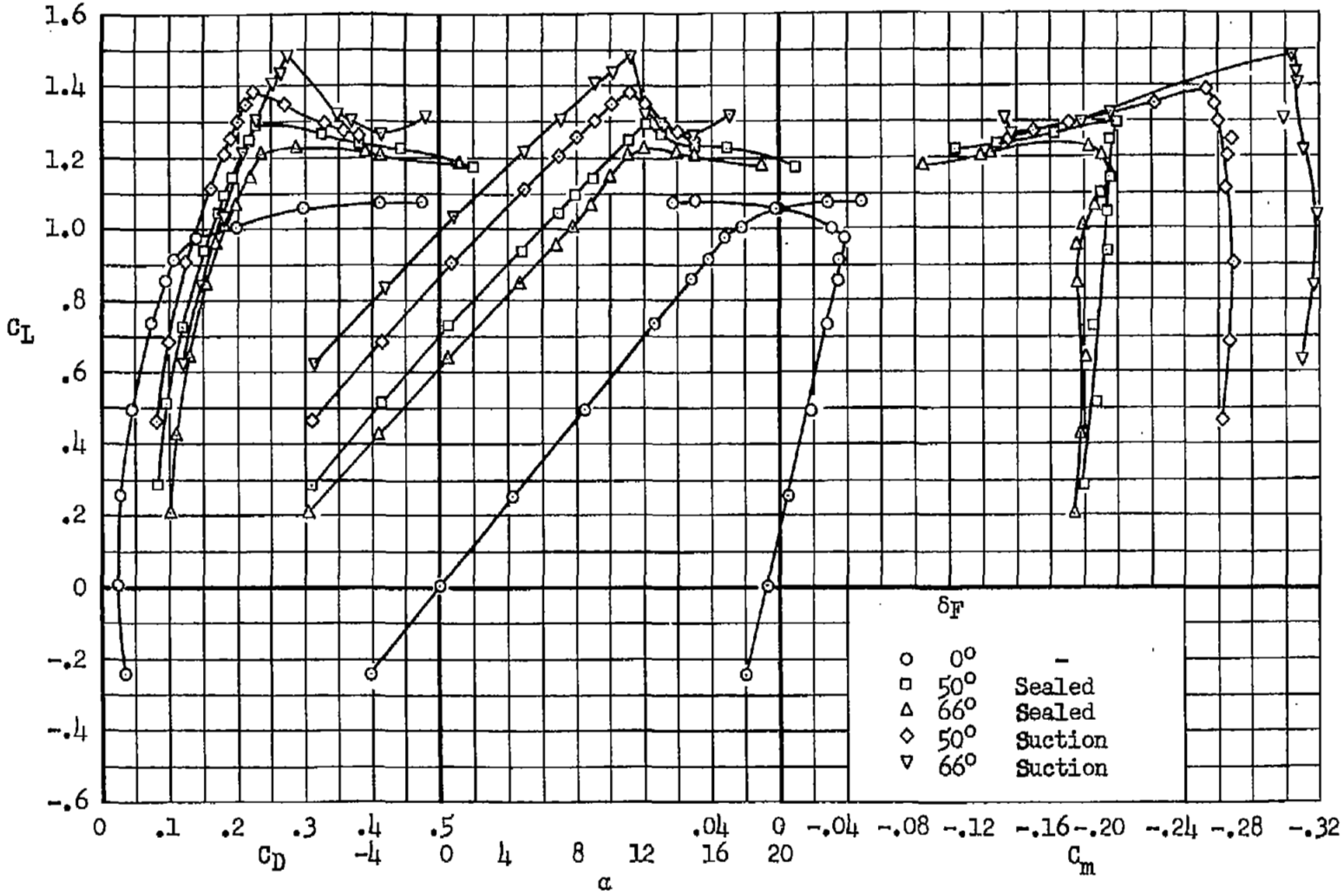

(b) Flap span; η_F = 0.16 to 0.75.

Figure 6.- Concluded.

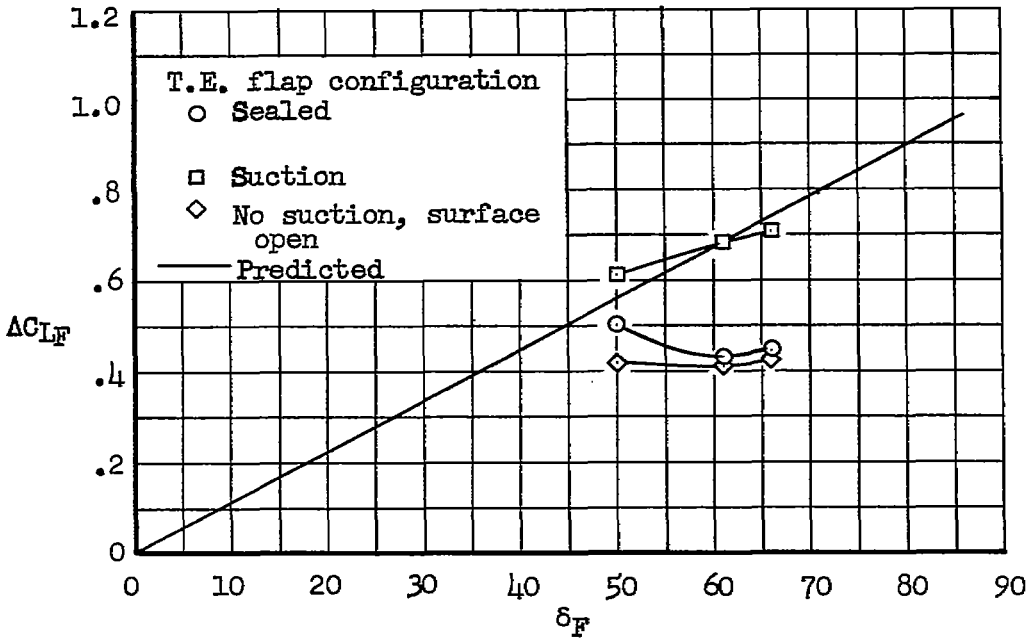

(a) η_F = 0.16 to 0.50

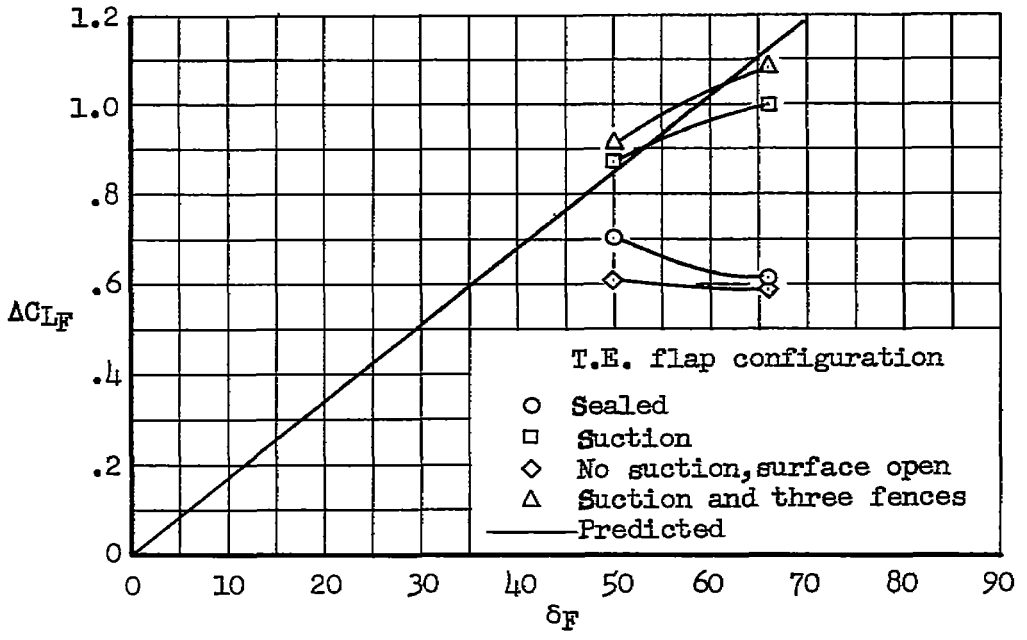

(b) η_F = 0.16 to 0.75

Figure 7.- Comparison of measured trailing-edge flap lift increments with theoretical values for $\alpha = 0.6^\circ$; $\delta_N = 0$, horizontal tail off, U = 156 ft/sec.

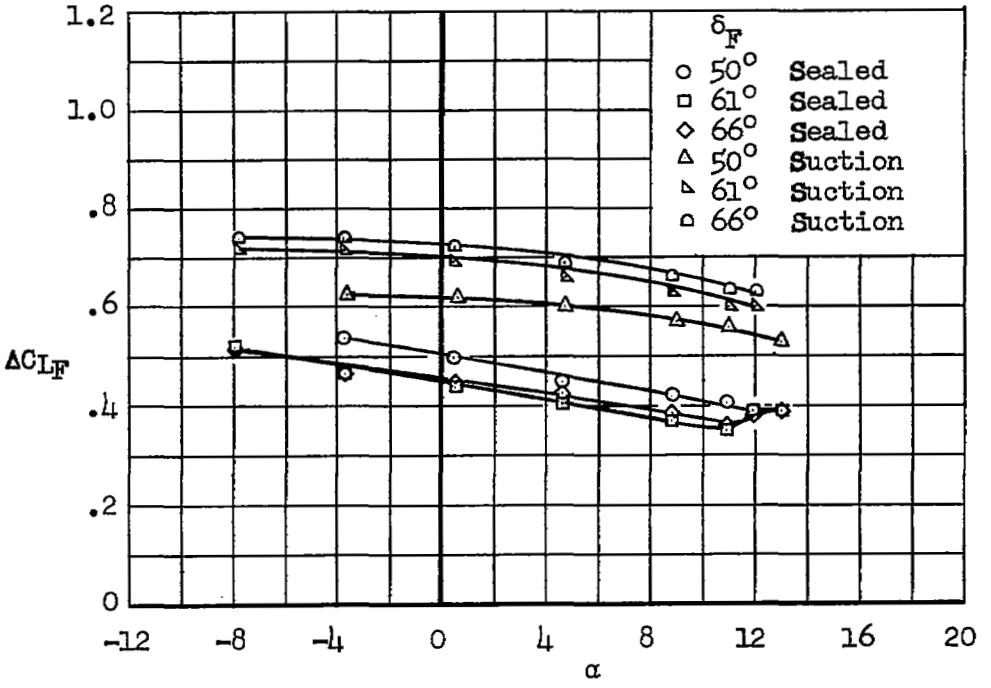

(a) η_F = 0.16 to 0.50

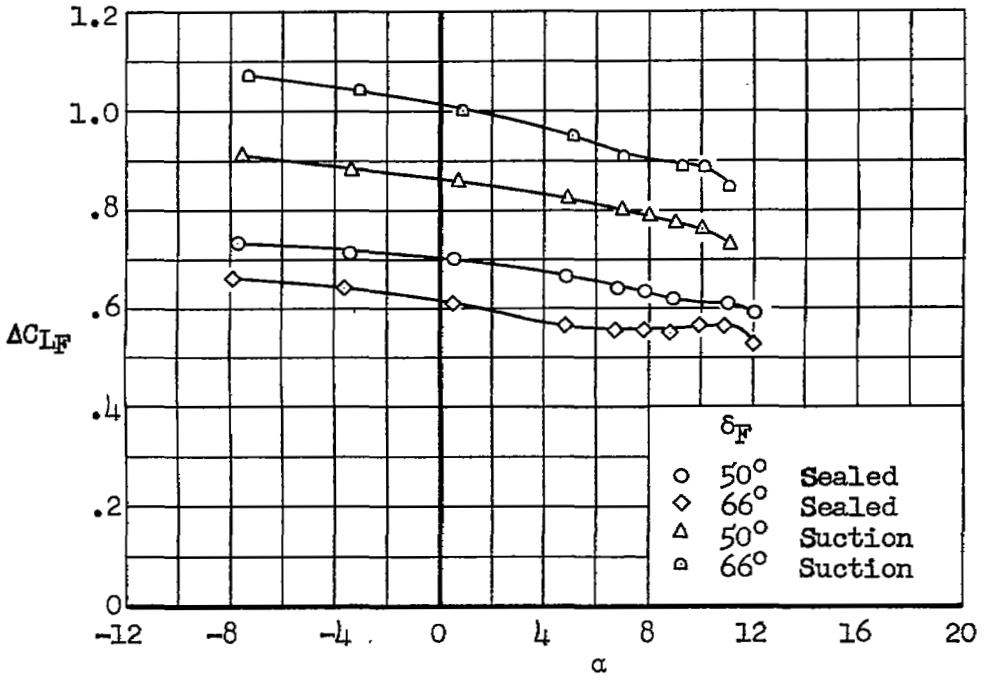

(b) η_F = 0.16 to 0.75

Figure 8.- Variation of trailing-edge flap lift increment with angle of attack; δ_N = 0°, horizontal tail off, U = 156 ft/sec.

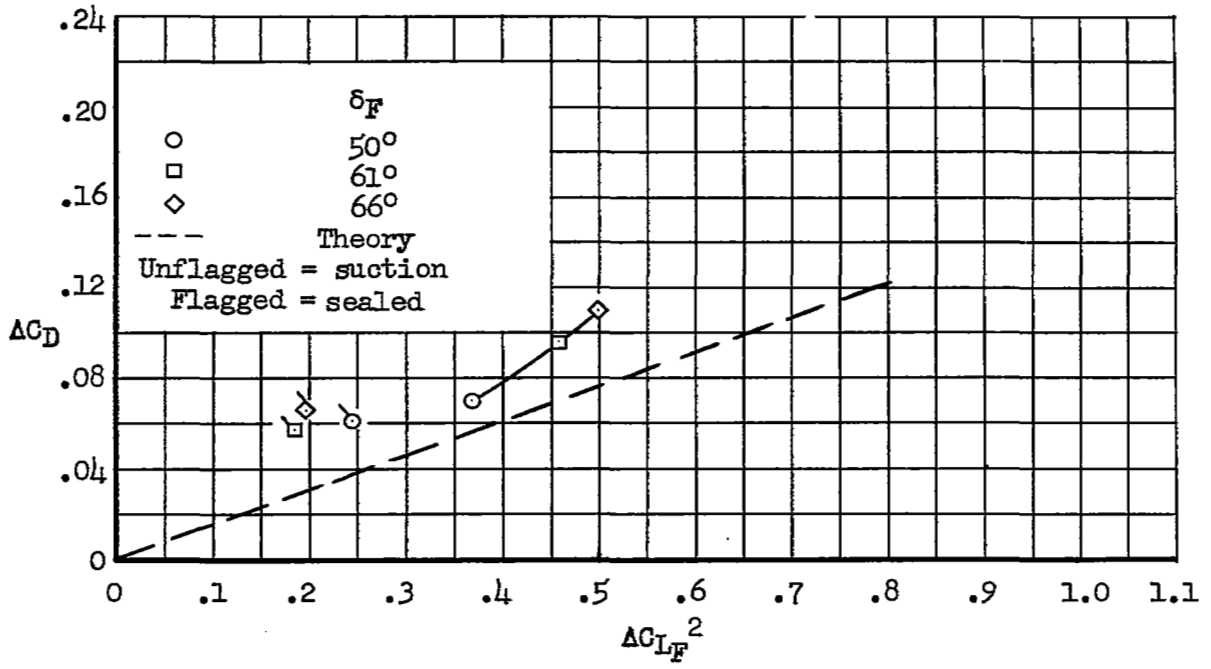

(a) η_F = 0.16 to 0.50

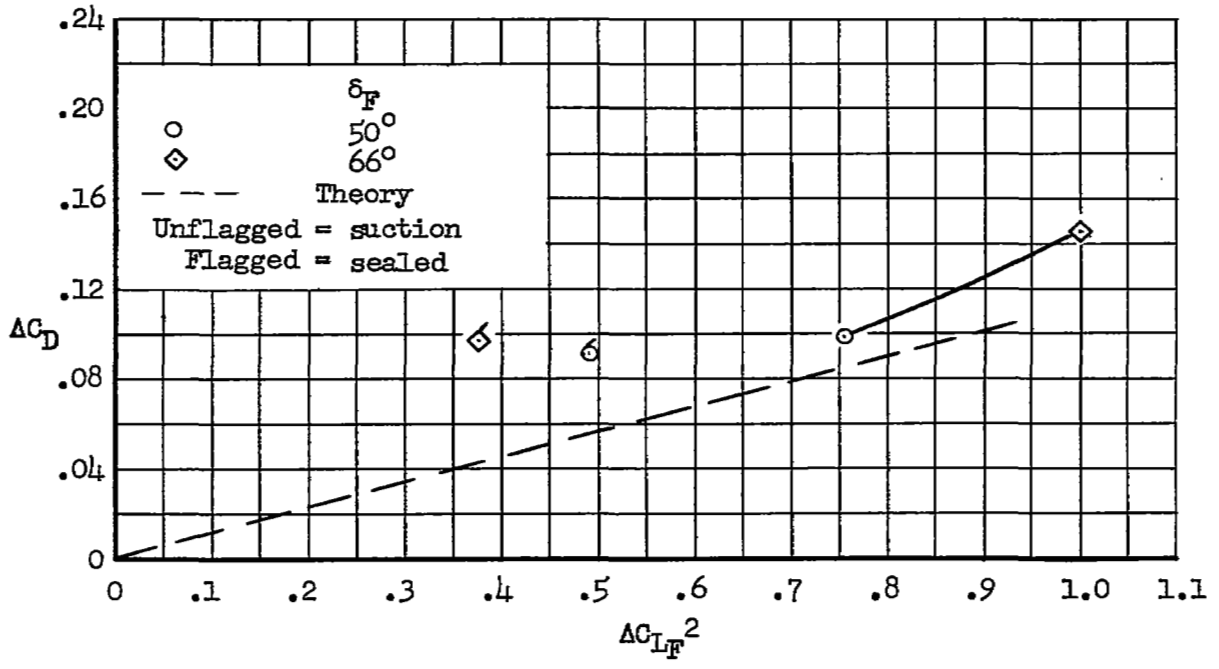

(b) η_F = 0.16 to 0.75

Figure 9.- Variation of drag increment with flap lift increment squared at 0° angle of attack; δ_N = 0°, horizontal tail off, U = 156 ft/sec.

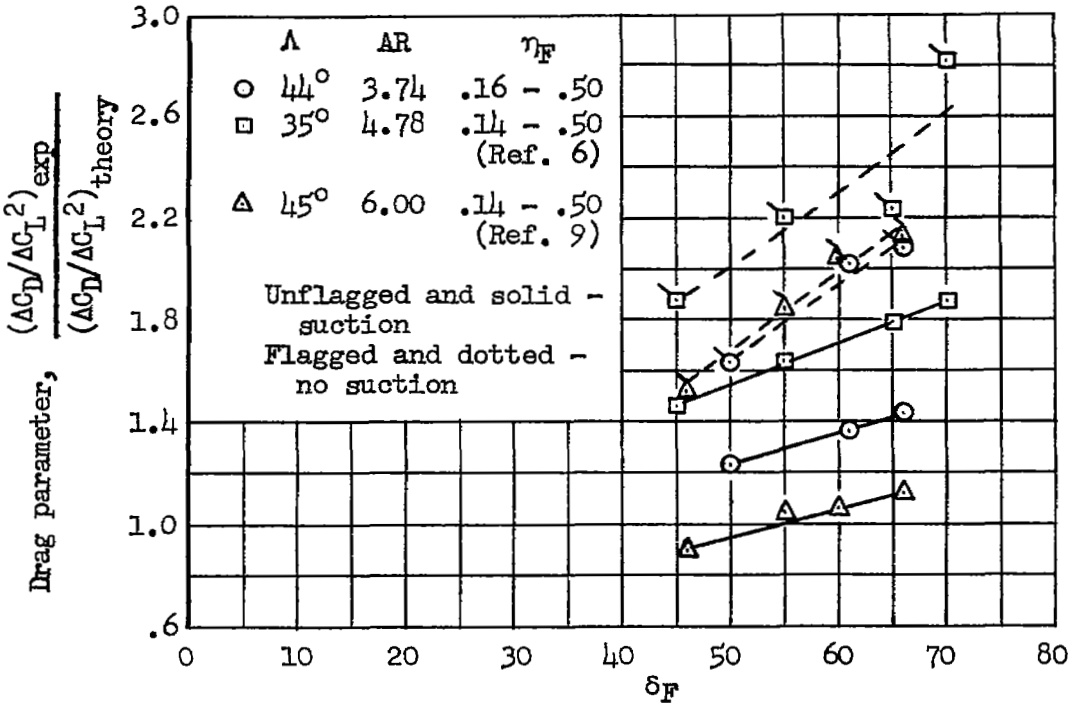

(a) η_F ~ 0.16 to 0.50

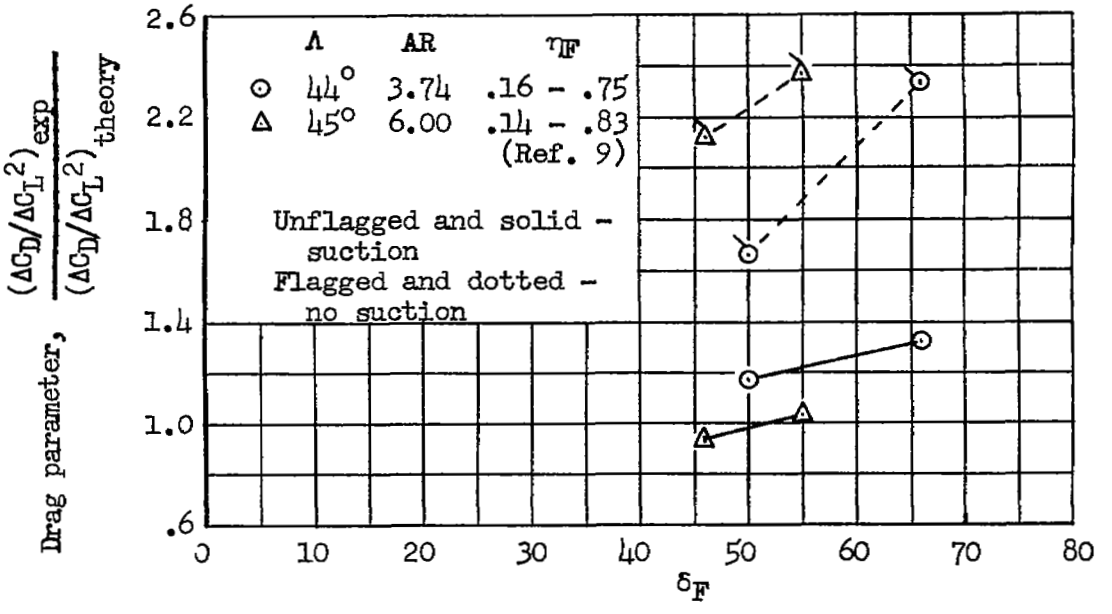

(b) η_F ~ 0.16 to 0.75

Figure 10.- Effect of flap deflection and suction on drag parameter (ratio of experimental to theoretical drag per flap lift increment squared) $\delta_N = 0°$; horizontal tail off, $\alpha = 0°$.

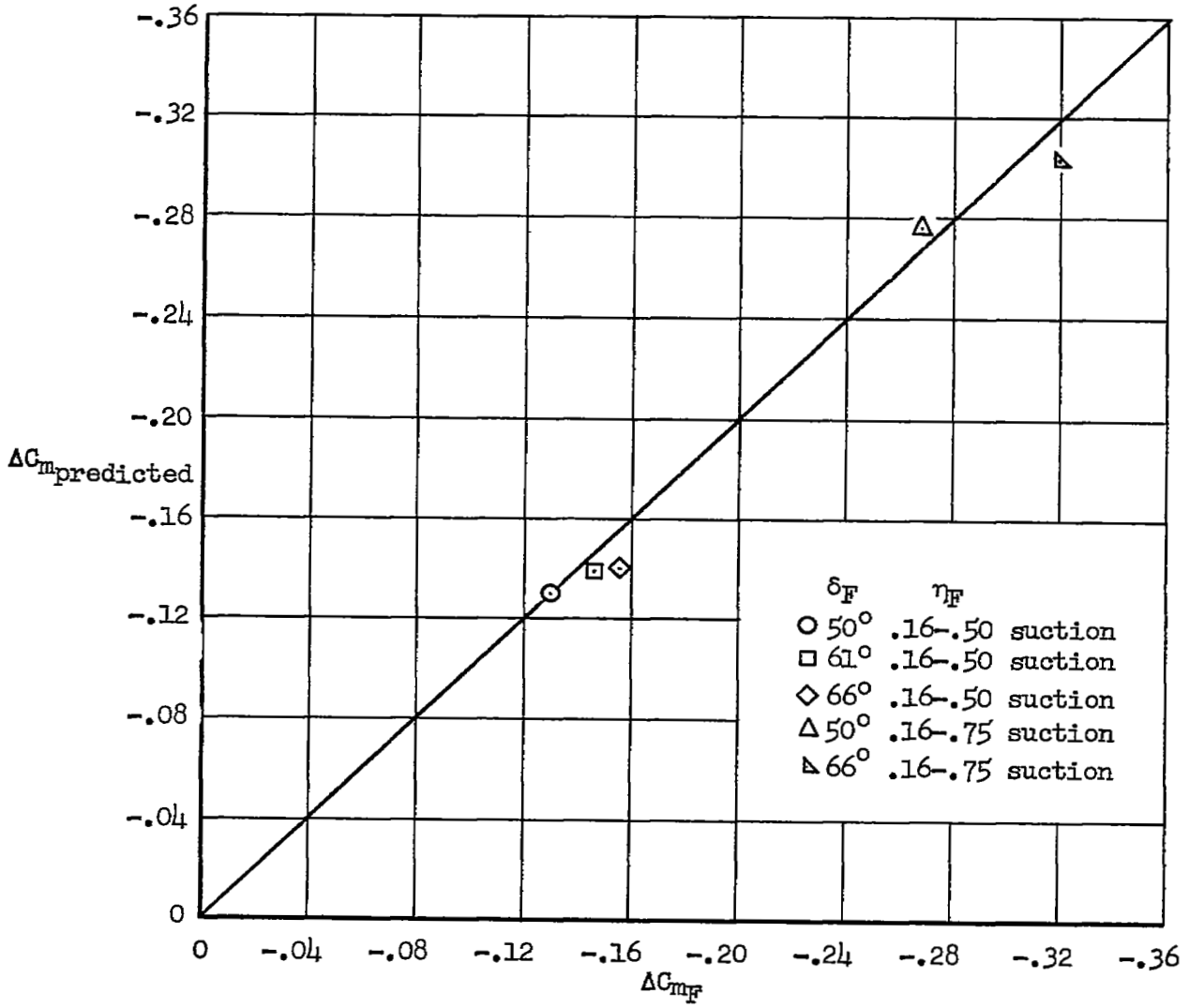

Figure 11.- Comparison of measured with predicted pitching-moment coefficients for area-suction trailing-edge flap; $\alpha = 0.6^\circ$, $U = 156$ ft/sec, $\delta_N = 0$, horizontal tail off.

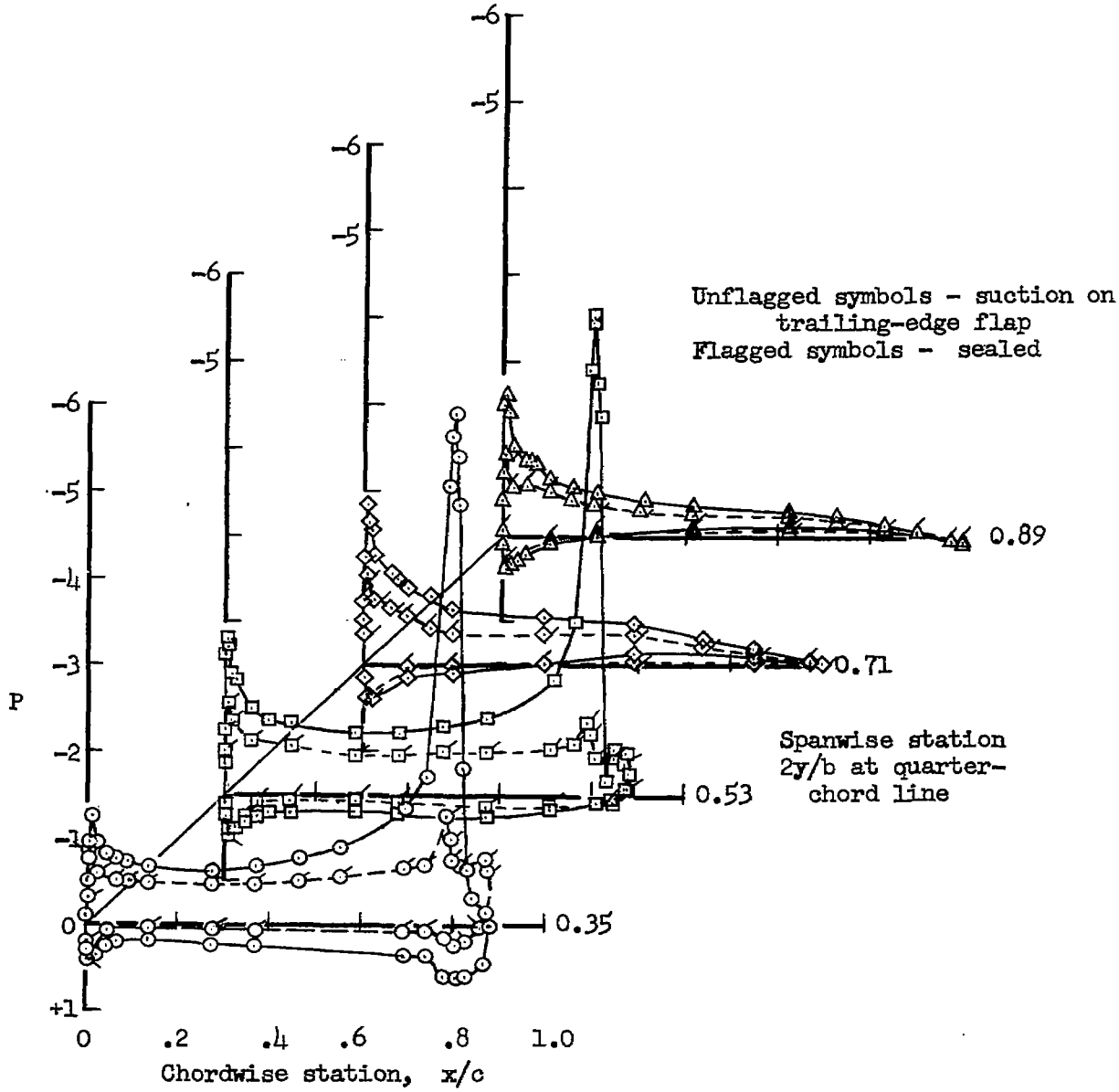

(a) $\alpha = 0.6^{\circ}$

Figure 12.- Chordwise pressure distribution for 66° trailing-edge flap with $\eta_F = 0.16$ to 0.50; $\delta_N = 0^{\circ}$, U = 156 ft/sec.

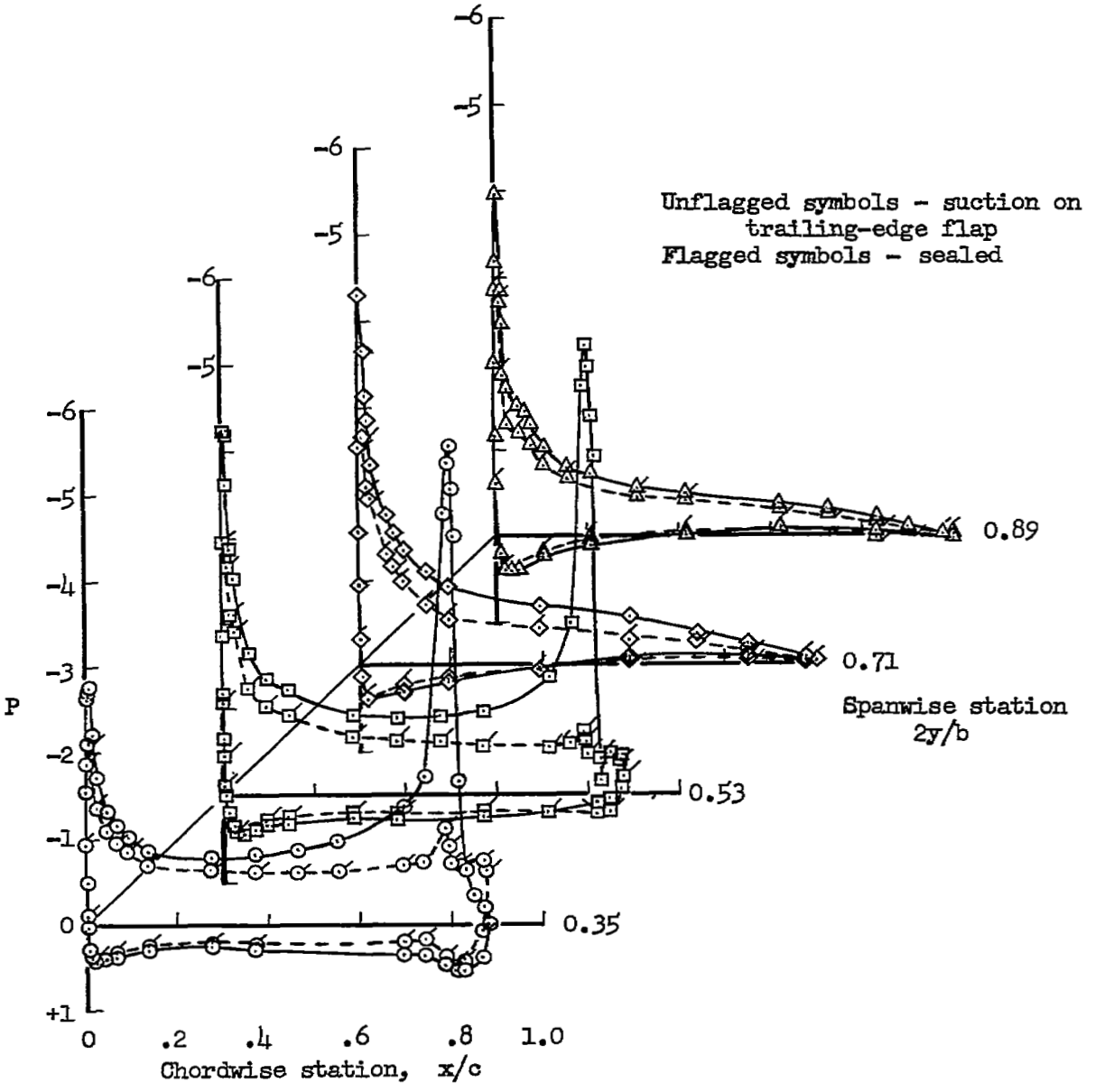

(b) $\alpha = 4.8^{\circ}$

Figure 12.- Continued.

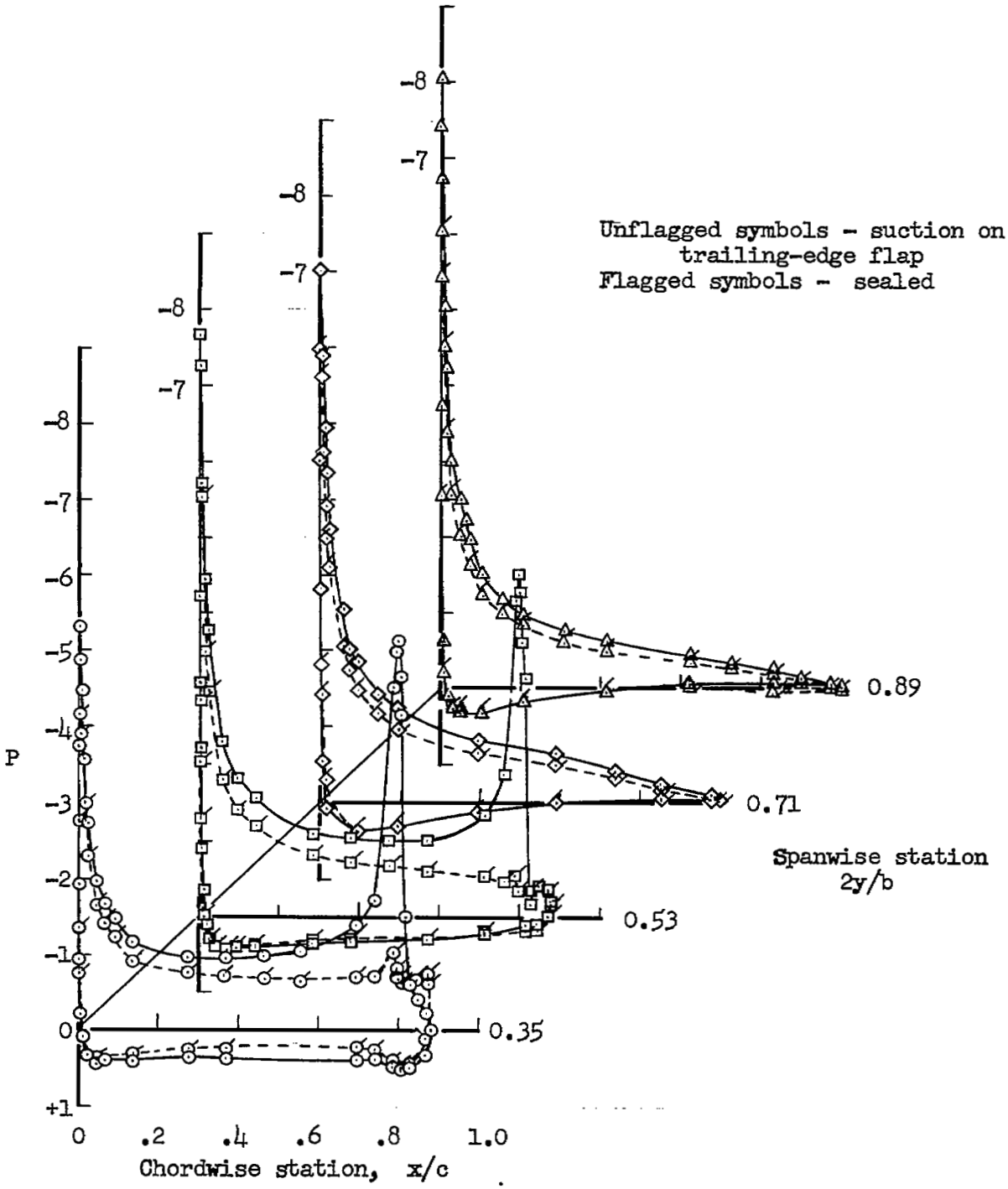

(c) $\alpha = 8.9^\circ$

Figure 12.- Continued.

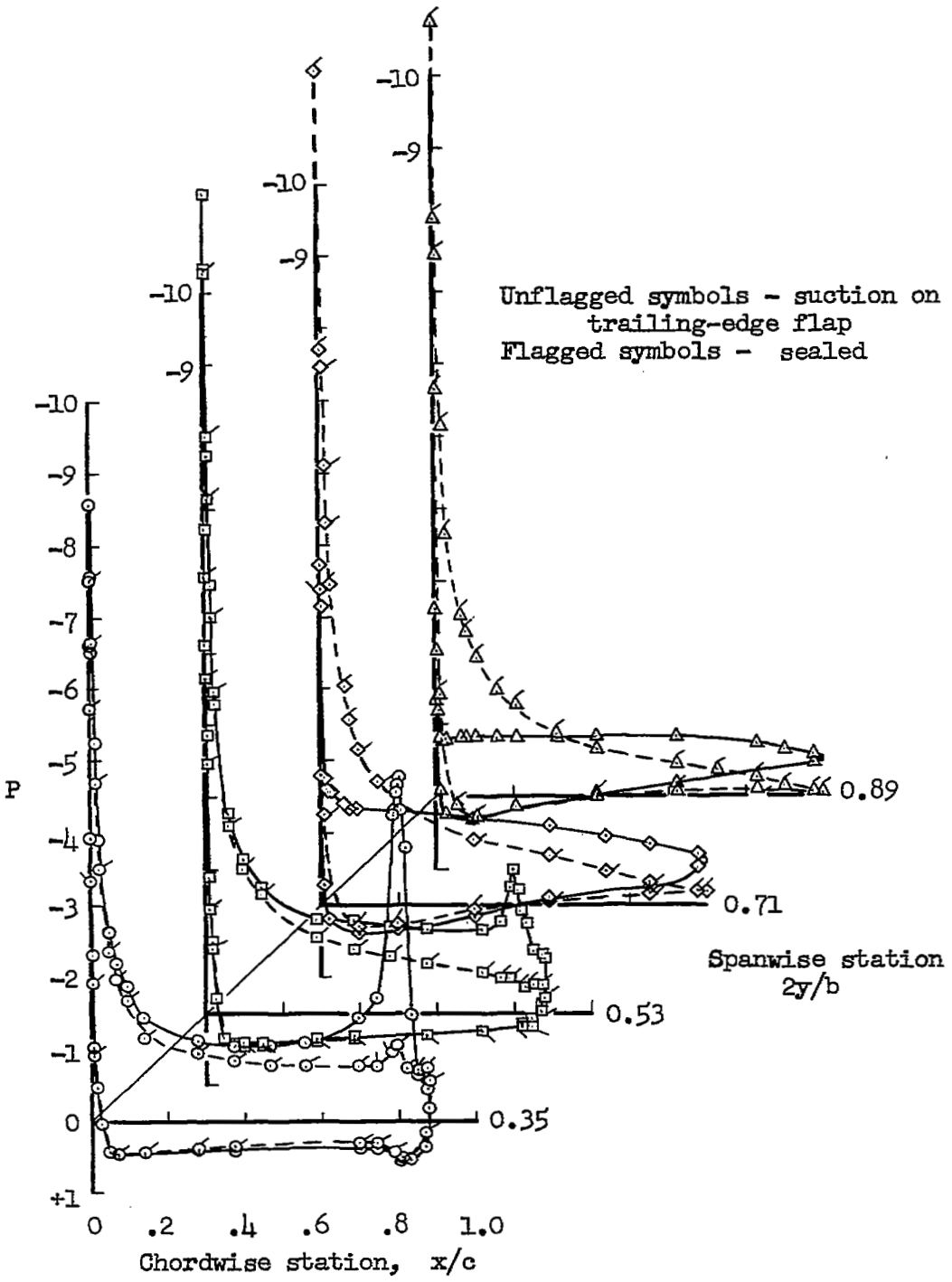

(d) $\alpha = 13.0^{\circ}$

Figure 12.- Continued.

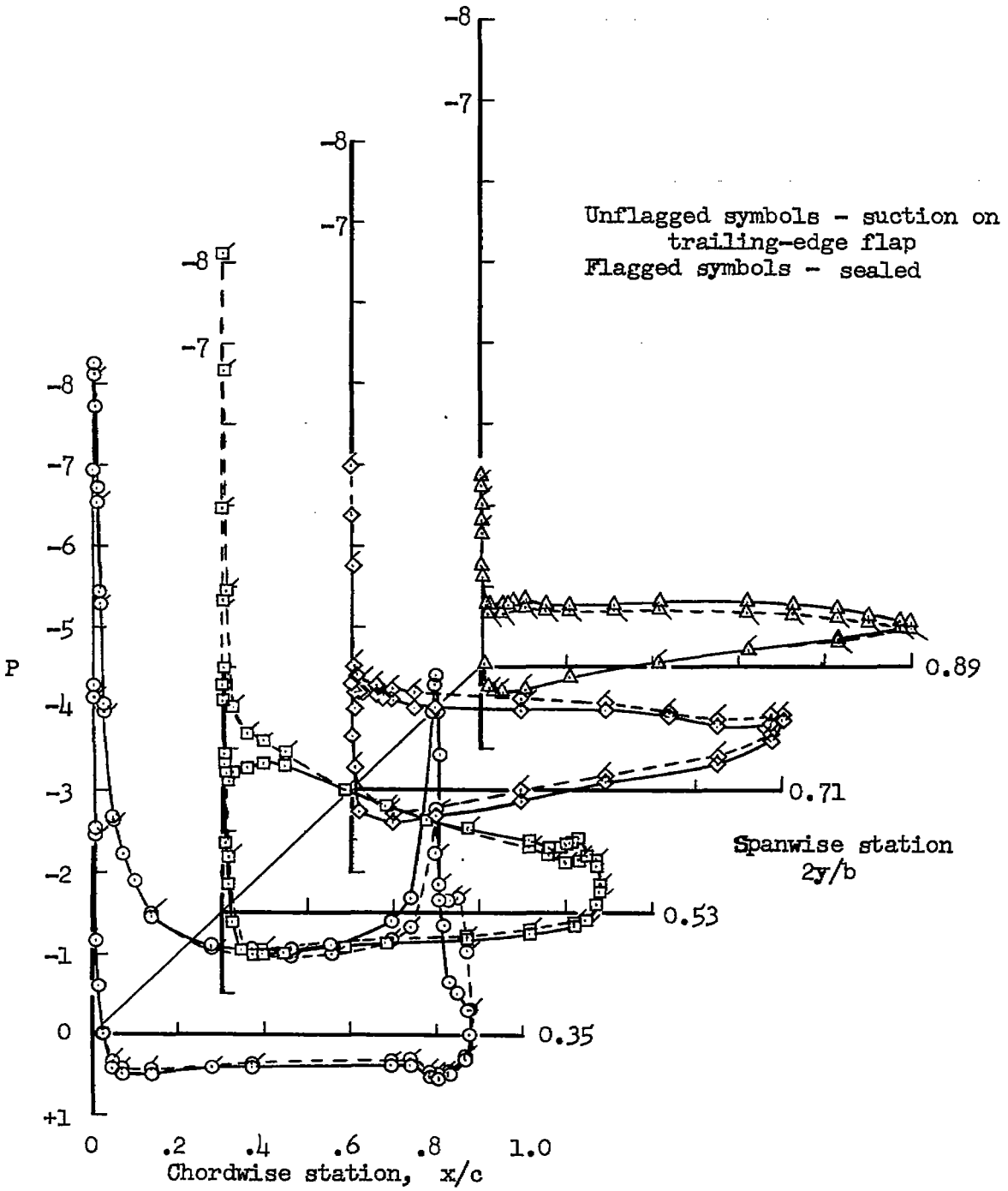

(e) $\alpha = 13.9^{\circ}$

Figure 12.- Concluded.

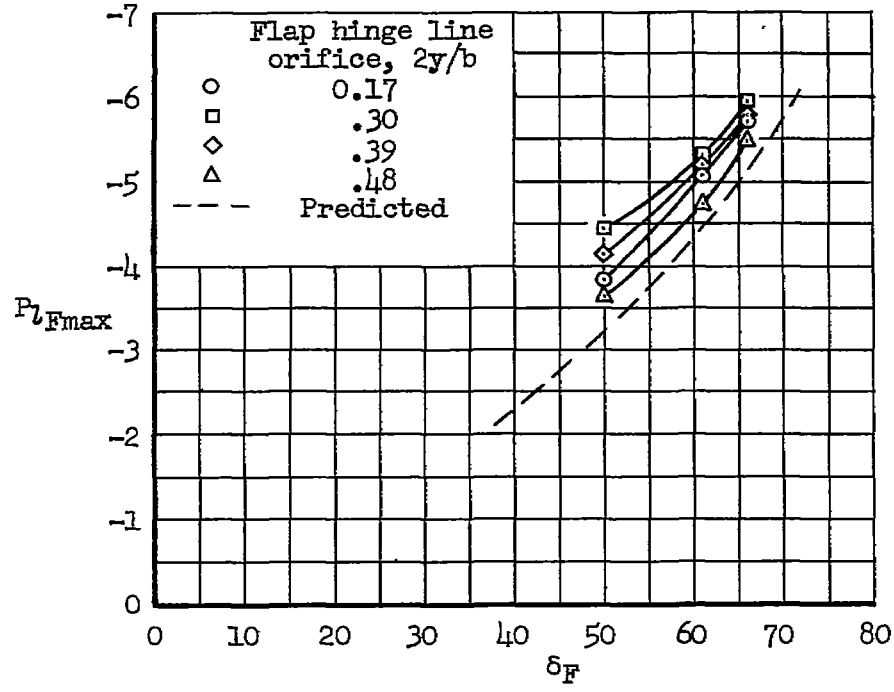

(a) η_F = 0.16 to 0.50

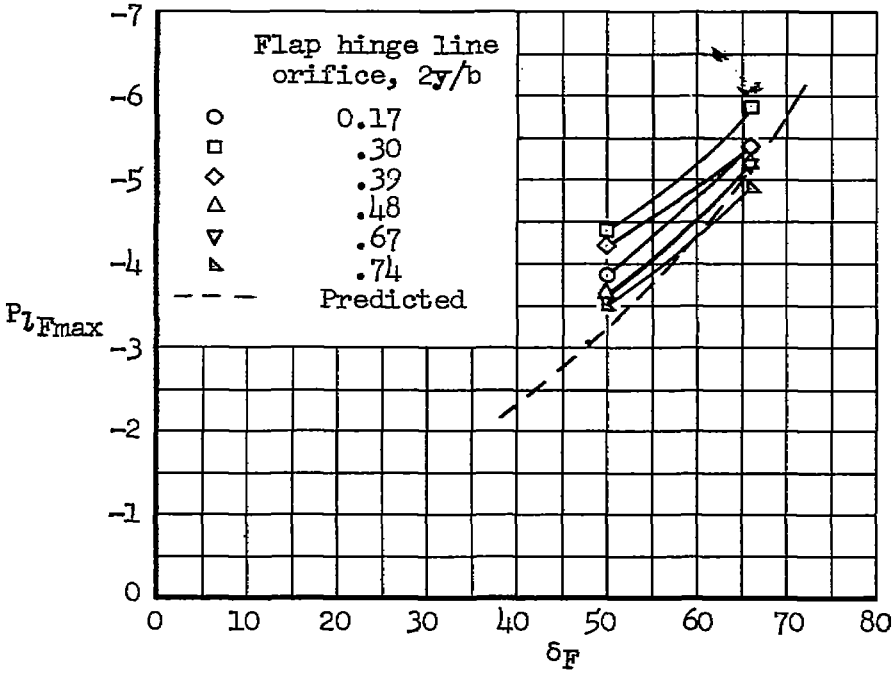

(b) η_F = 0.16 to 0.75

Figure 13.- Comparison of peak surface pressure coefficient on suction trailing-edge flap with values predicted; $\delta_N = 0^\circ$, $\alpha = 0.6^\circ$, U = 156 ft/sec.

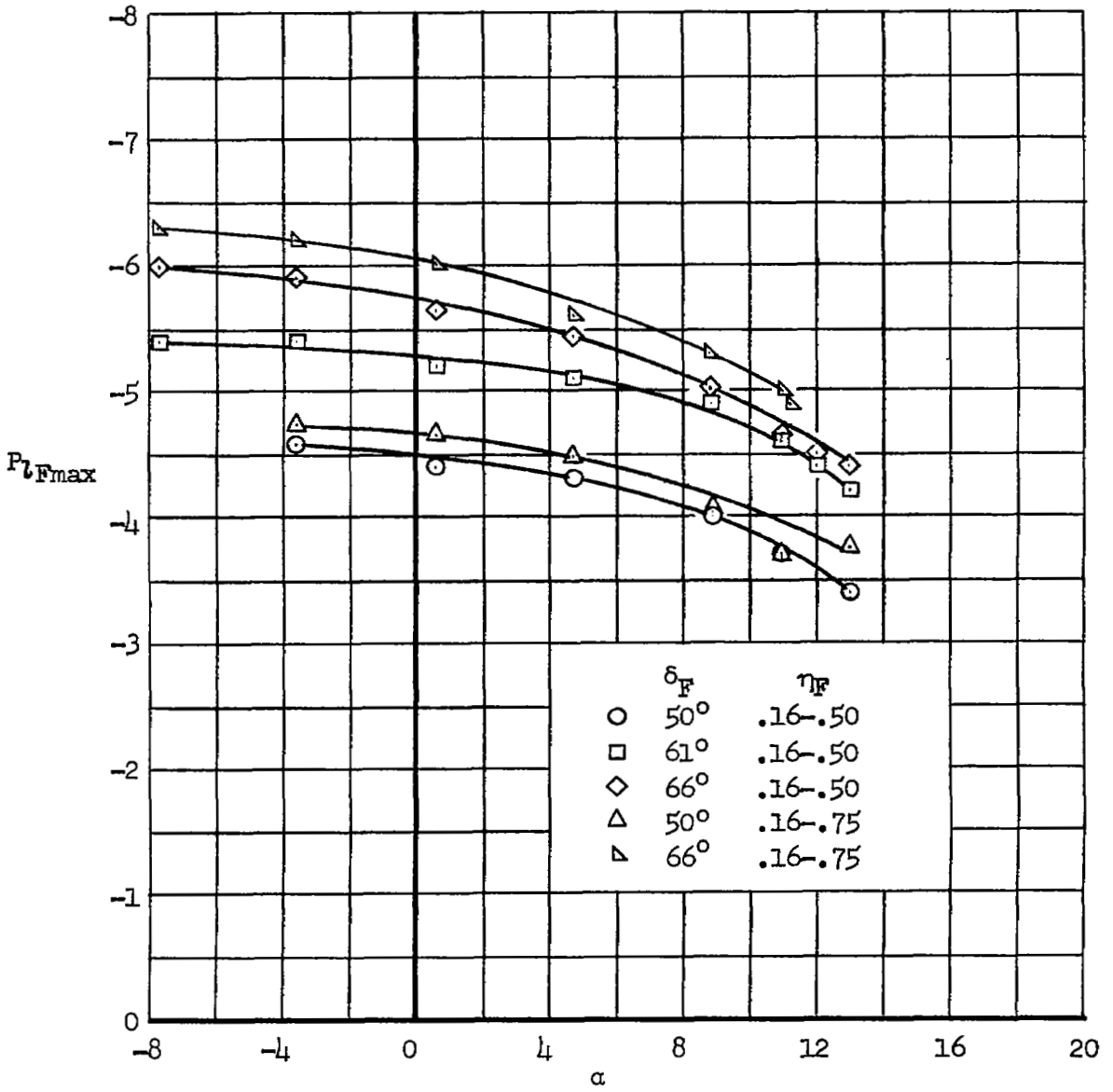

Figure 14.- Variation with angle of attack of the peak pressure coefficient on area-suction trailing-edge flap at 2y/b = 0.30; $\delta_N = 0°$, U = 156 ft/sec.

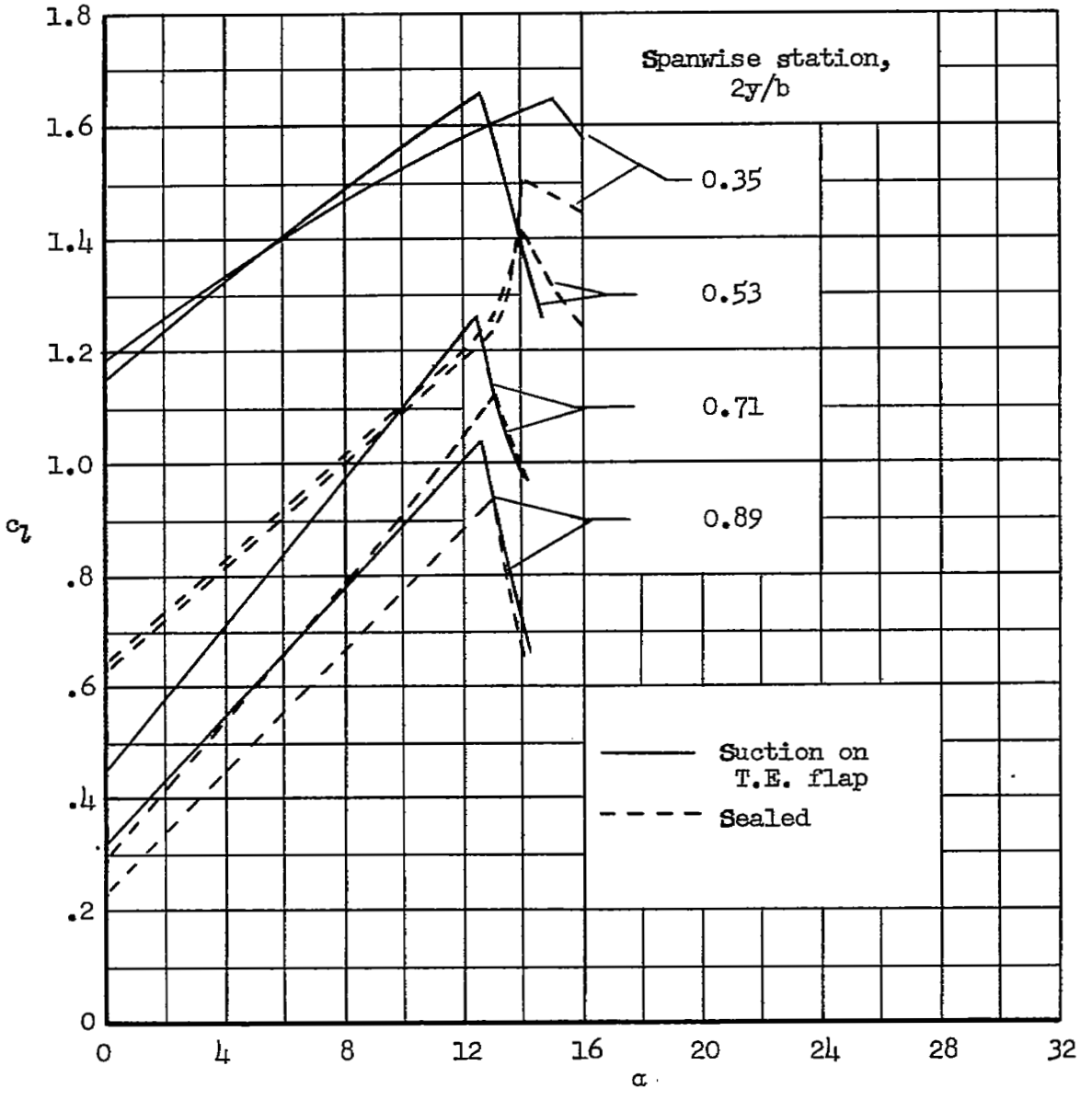

Figure 15.- Variation of section lift coefficient with angle of attack; $\delta_F = 66^\circ$, $\eta_F = 0.16$ to 0.50, $\delta_N = 0$, U = 156 ft/sec.

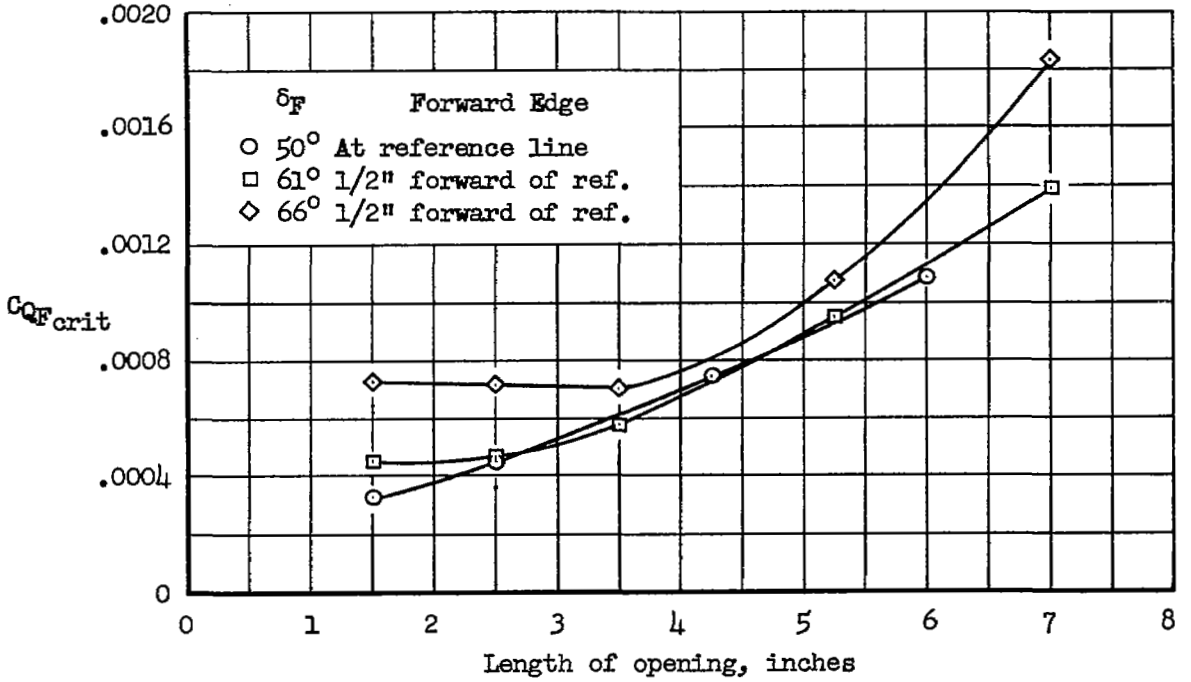

(a) Porous surface extent.

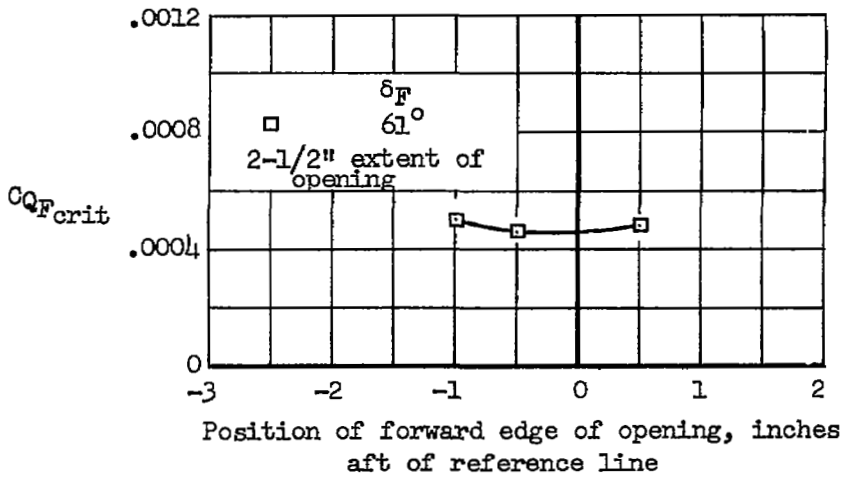

(b) Porous surface position.

Figure 16.- Variation of flow coefficient with extent and position of opening; η_F = 0.16 to 0.50, α = 0.6°, U = 156 ft/sec.

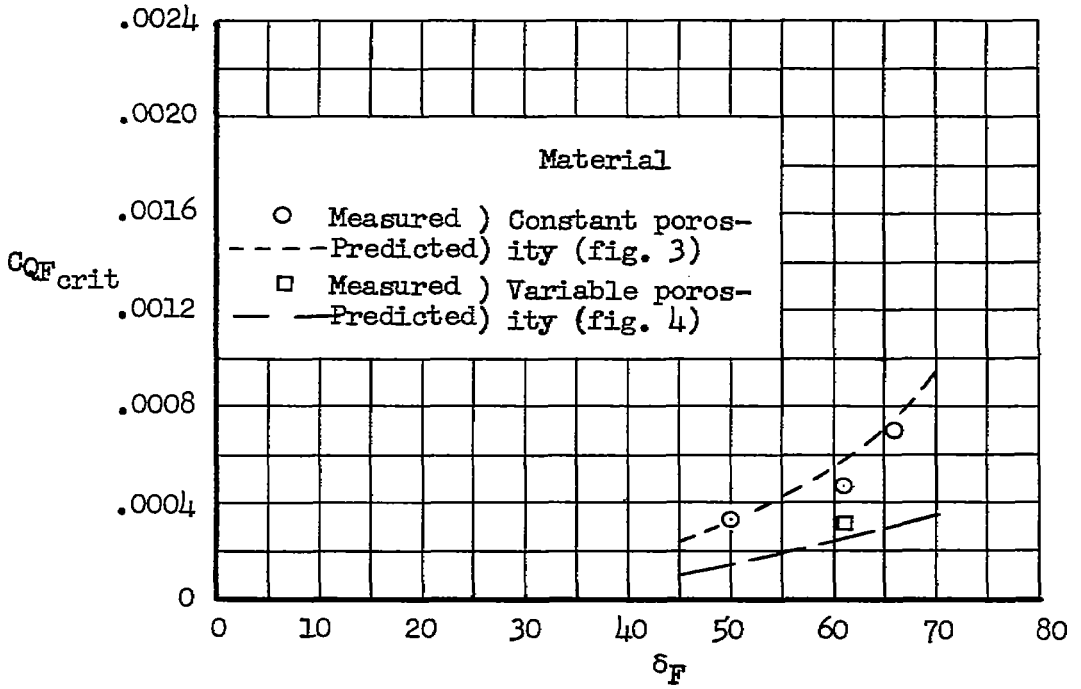

(a) η_F = 0.16 to 0.50

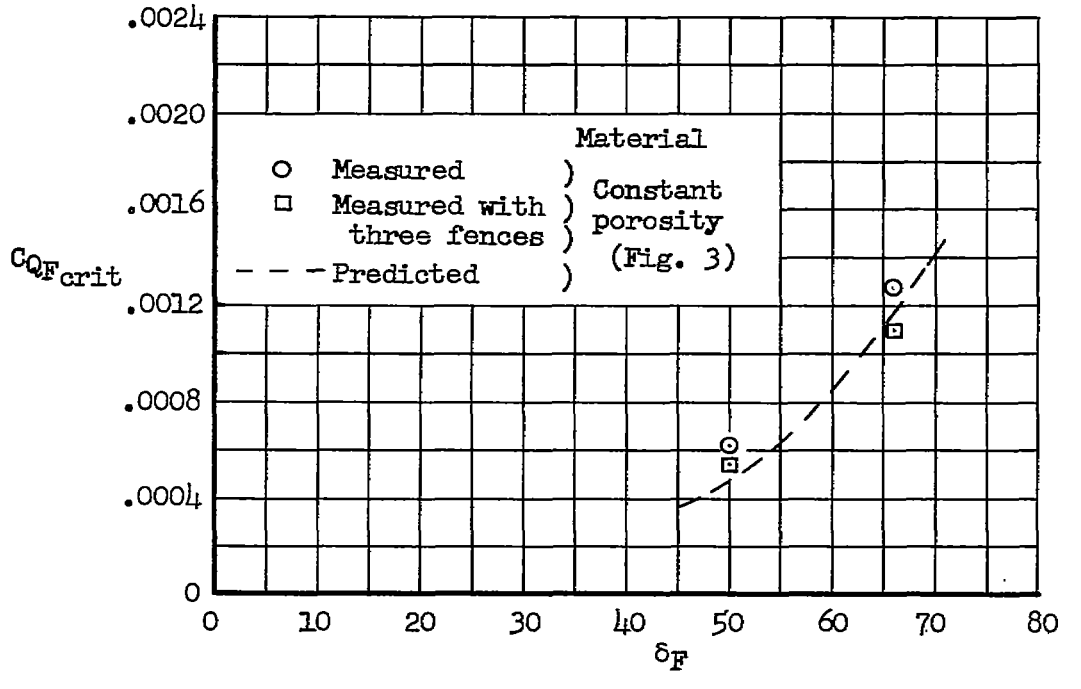

(b) η_F = 0.16 to 0.75

Figure 17.- Comparison of measured flow coefficients for trailing-edge flap with those predicted; $\alpha = 0.6^\circ$, U = 156 ft/sec, $\delta_N = 0^\circ$.

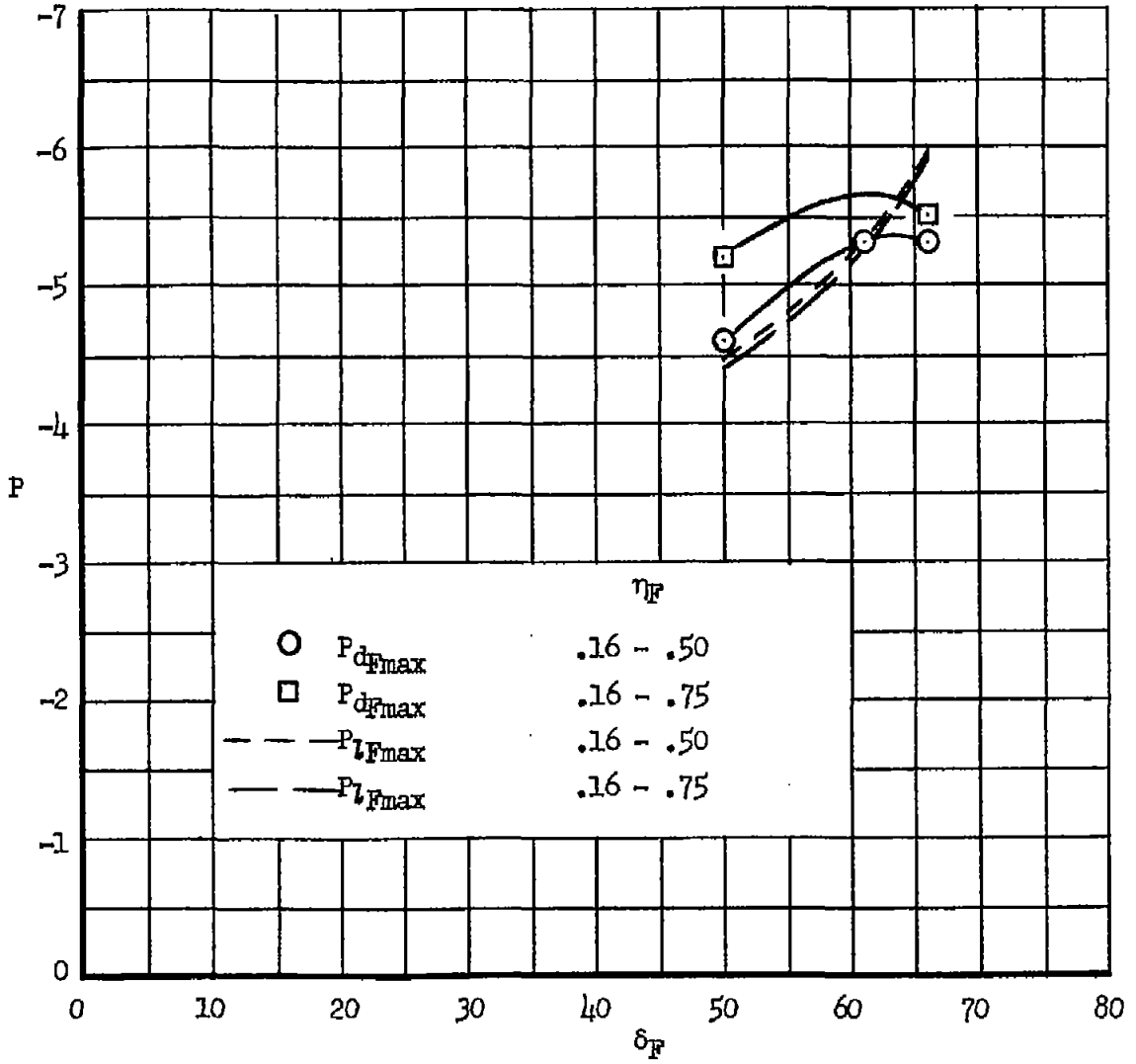

Figure 18.- Comparison of duct pressure coefficient with peak external pressure coefficient on suction trailing-edge flap; $\alpha = 0.6^\circ$, U = 156 ft/sec, $\delta_N = 0^\circ$.

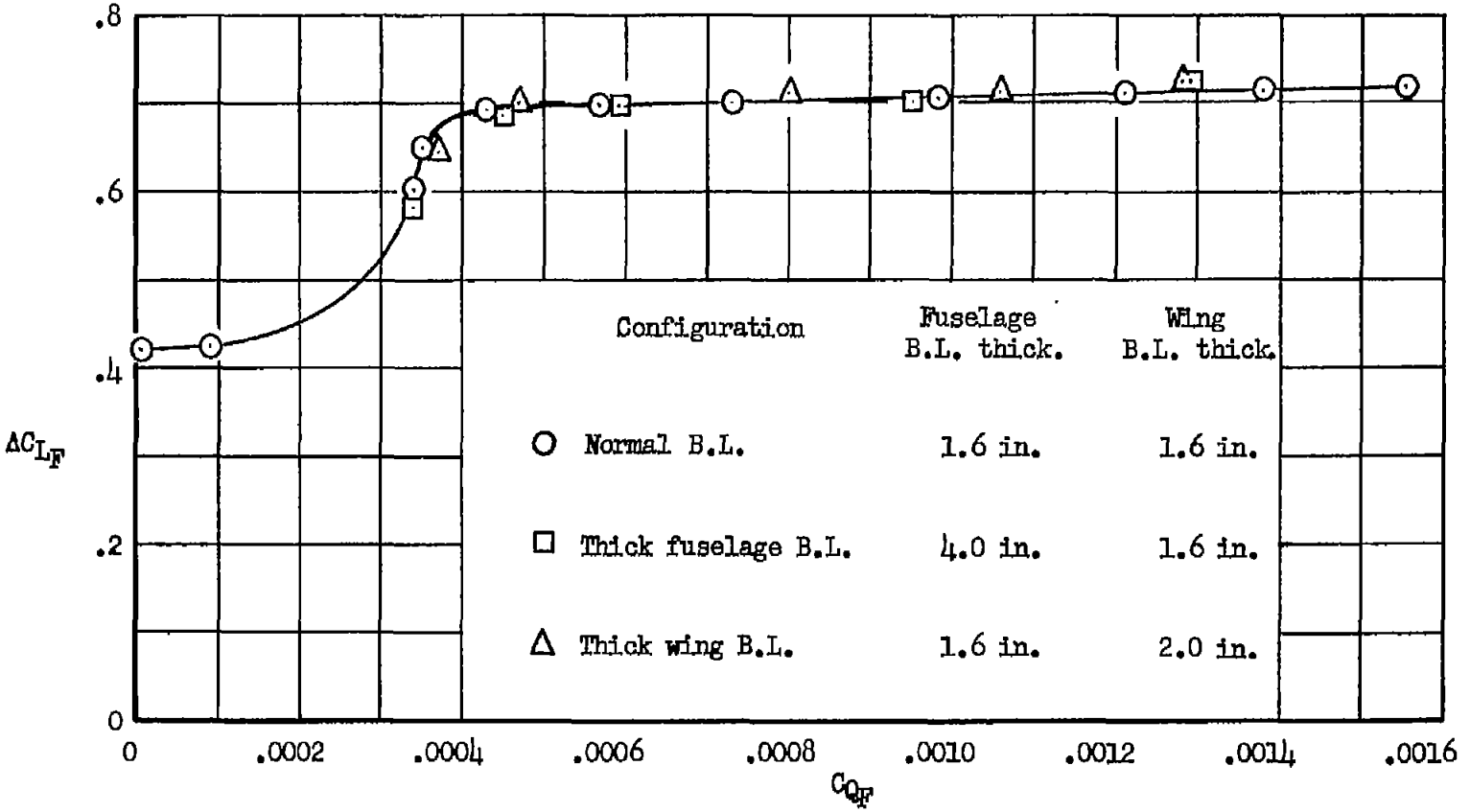

Figure 19.- Effect of boundary-layer thickness on flap lift increment and flow coefficient for $\delta_F = 61^\circ$; $\eta_F = 0.16$ to 0.50, $\delta_N = 0$, horizontal tail off, $\alpha = 0.6^\circ$, U = 156 ft/sec.

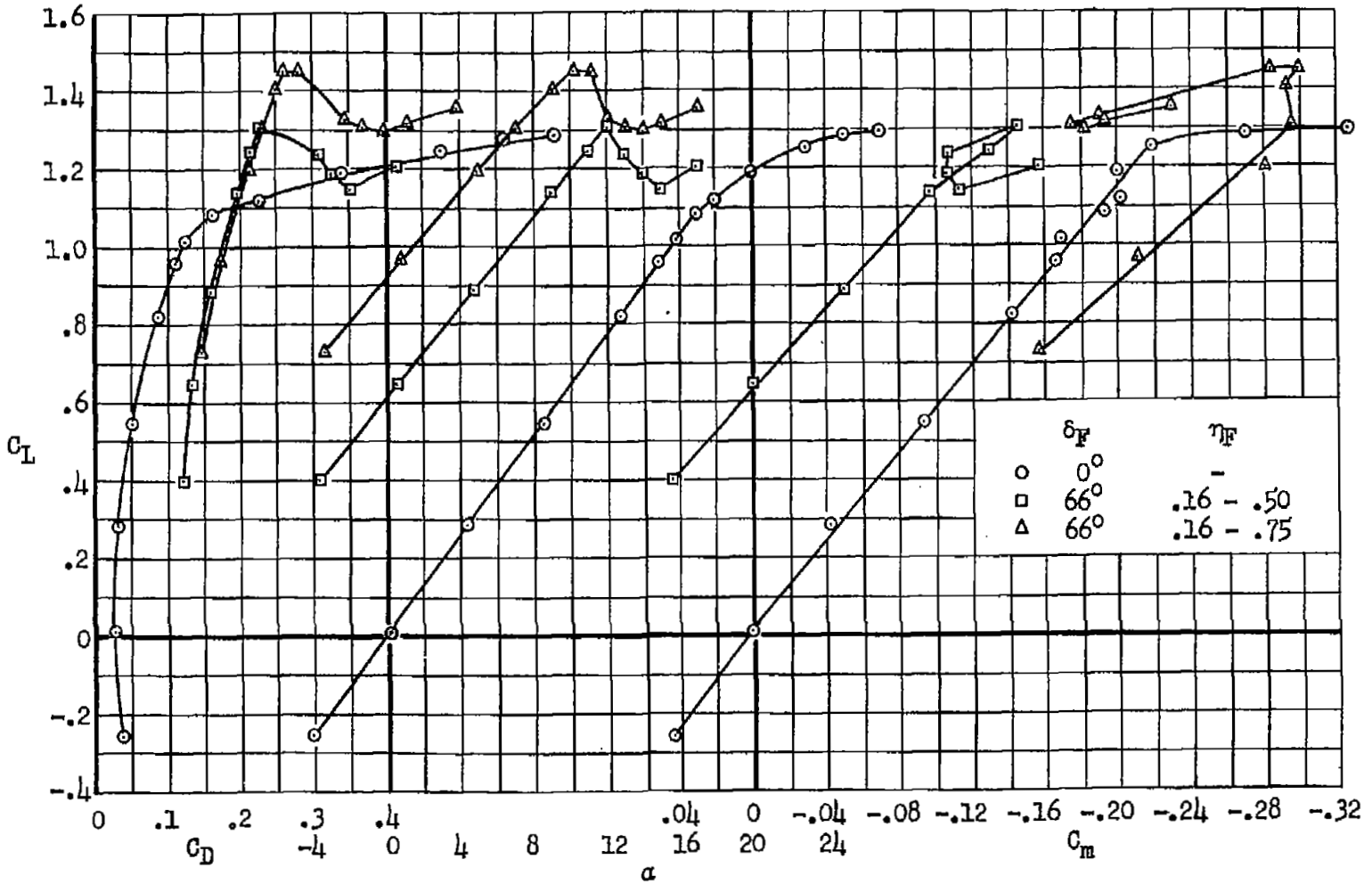

Figure 20.- Longitudinal characteristics of the model with horizontal tail on; $\delta_N = 0°$, U = 156 ft/sec.

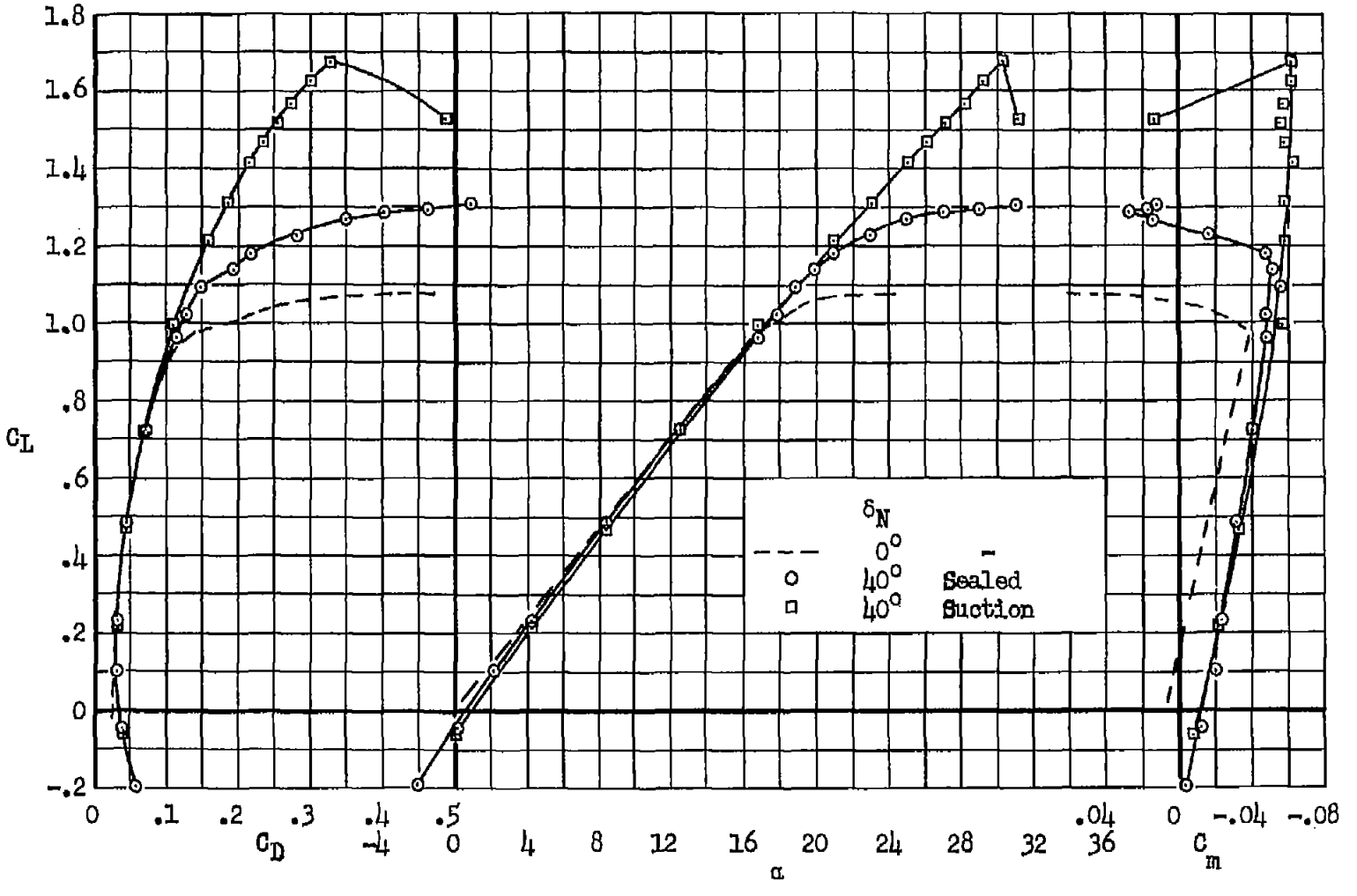

(a) $\delta_F = 0°$

Figure 21.- Longitudinal characteristics of the model with the nose flap deflected and several trailing-edge flap configurations; horizontal tail off, U = 156 ft/sec.

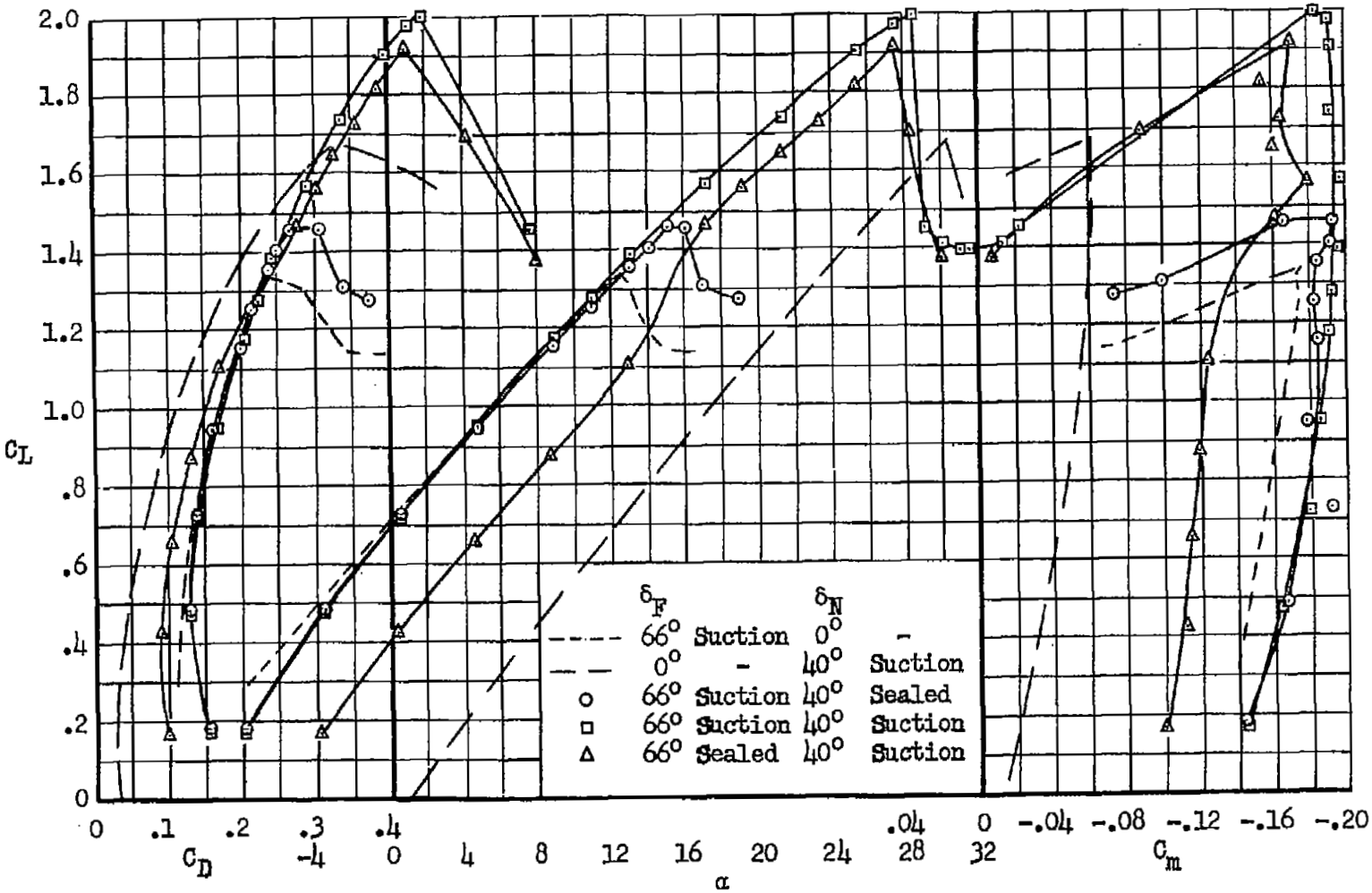

(b) $\delta_F = 66^\circ$, $\eta_F = 0.16$ to 0.50

Figure 21.- Continued.

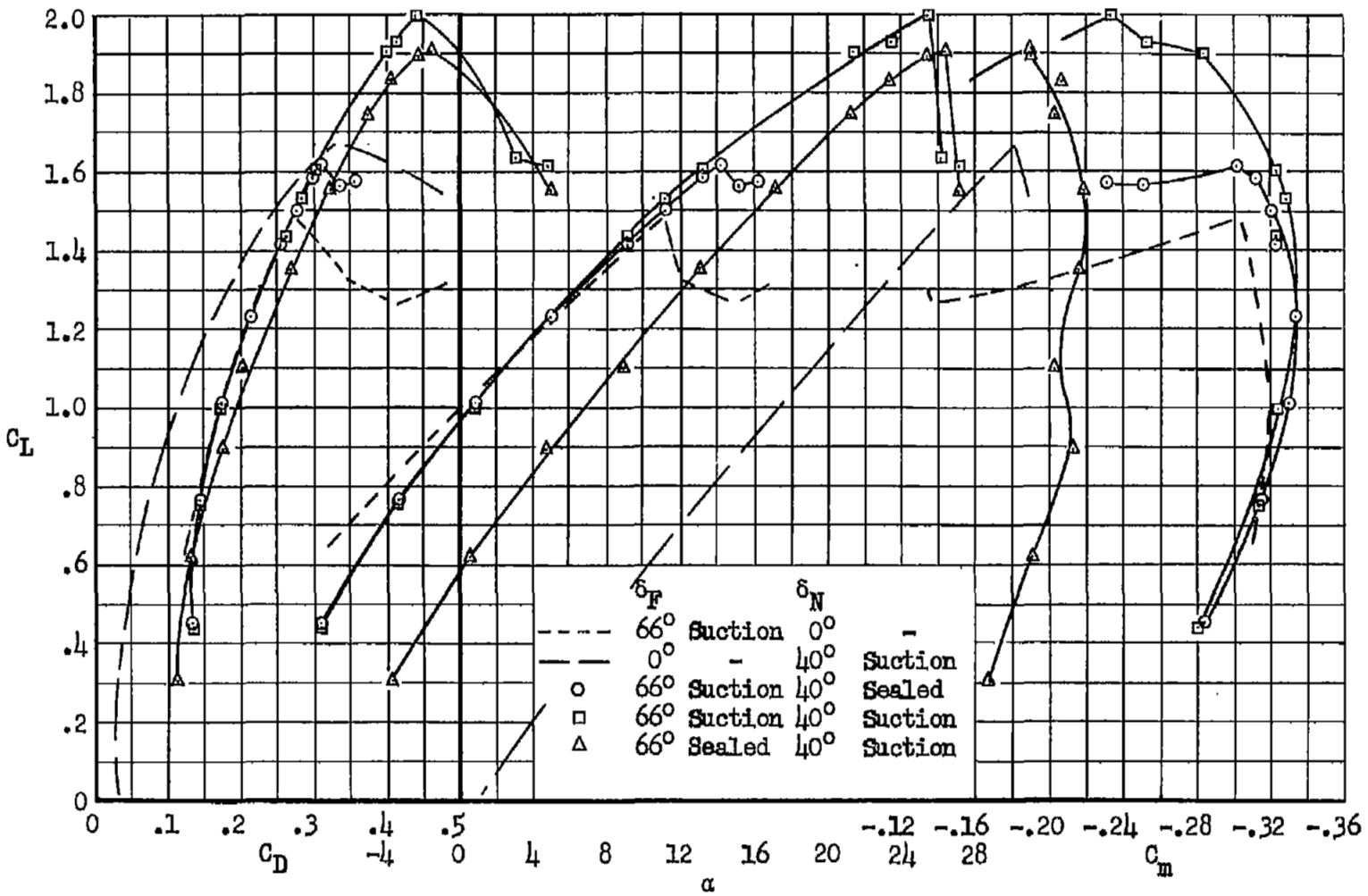

(c) $\delta_F = 66°$, $\eta_F = 0.16$ to 0.75

Figure 21.- Concluded.

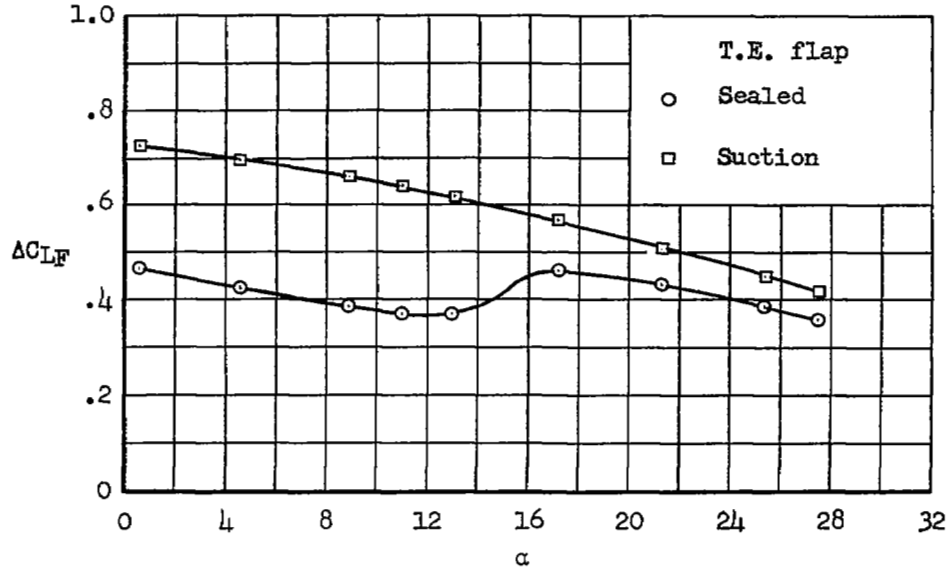

(a) $\delta_F = 66^\circ$, $\eta_F = 0.16$ to 0.50

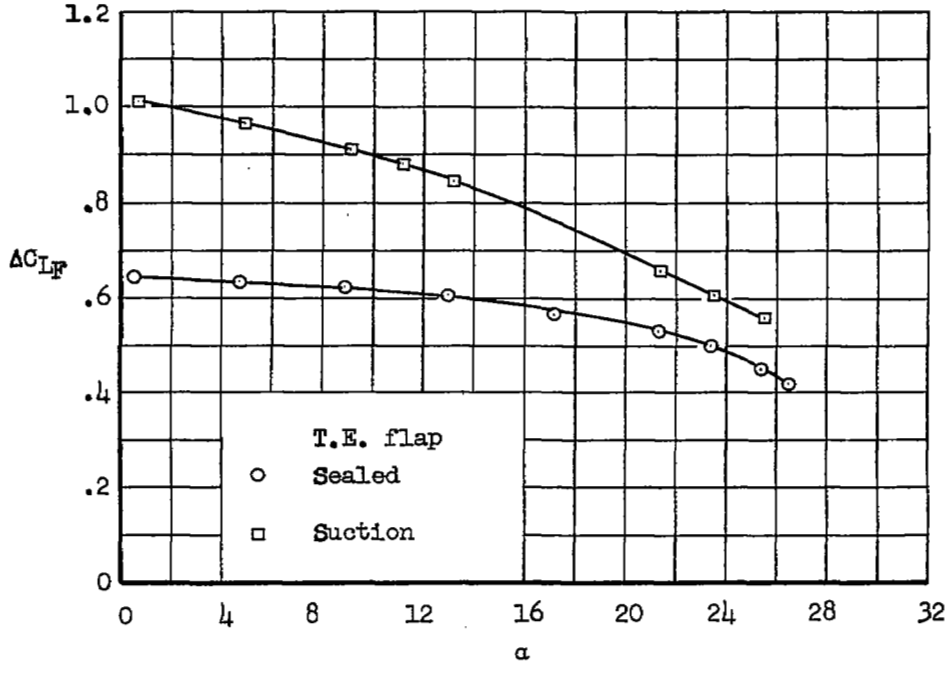

(b) $\delta_F = 66^\circ$, $\eta_F = 0.16$ to 0.75

Figure 22.- Variation of trailing-edge flap lift increment with angle of attack for model with 40° leading-edge area-suction flap; U = 156 ft/sec.

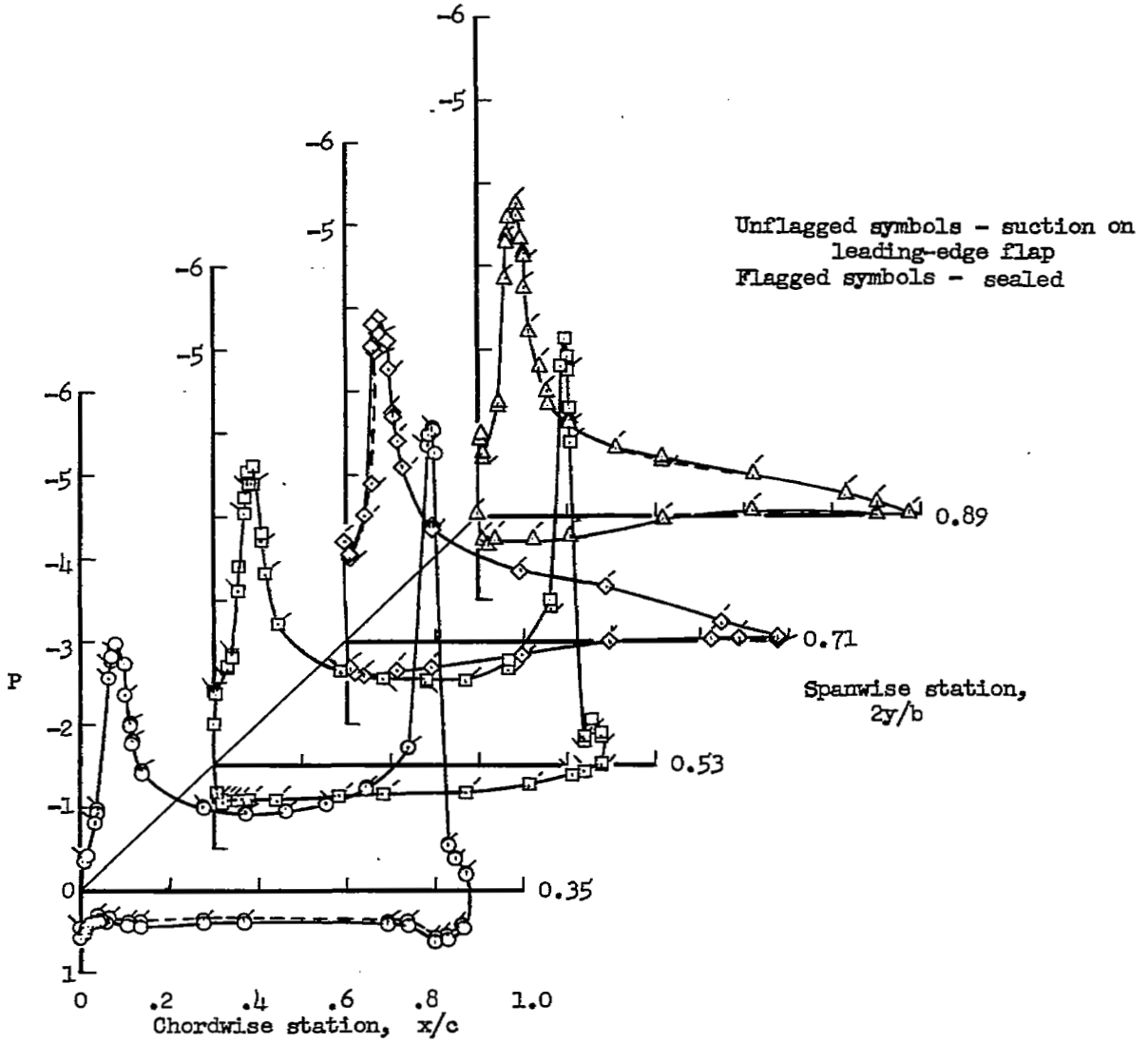

(a) $\alpha = 8.9^\circ$

Figure 23.- Chordwise pressure distributions with $\delta_N = 40^\circ$. Trailing-edge flap deflected 66°, $\eta_F = 0.16$ to 0.50 with suction applied; U = 156 ft/sec.

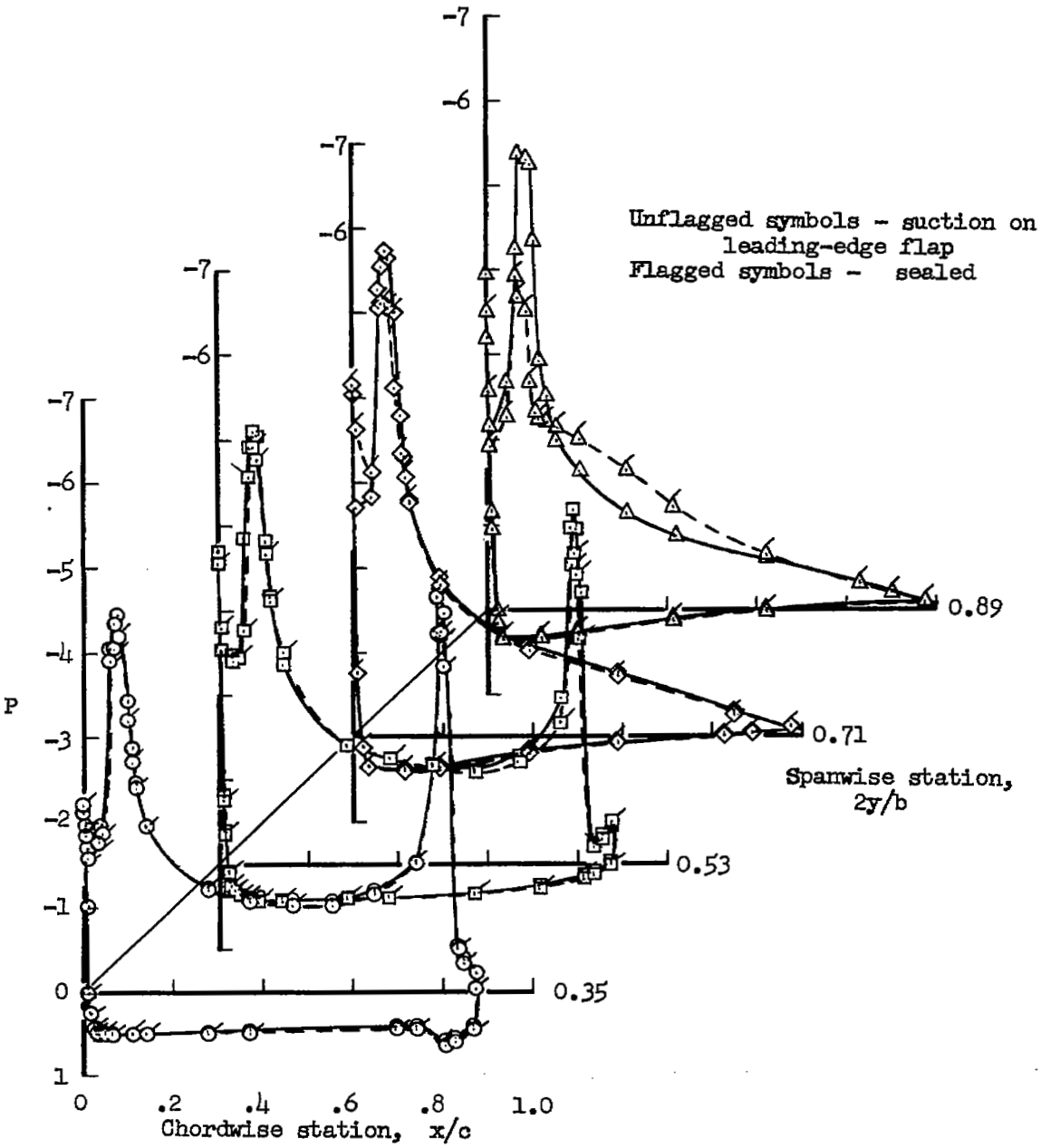

(b) $\alpha = 15.2^{\circ}$

Figure 23.- Continued.

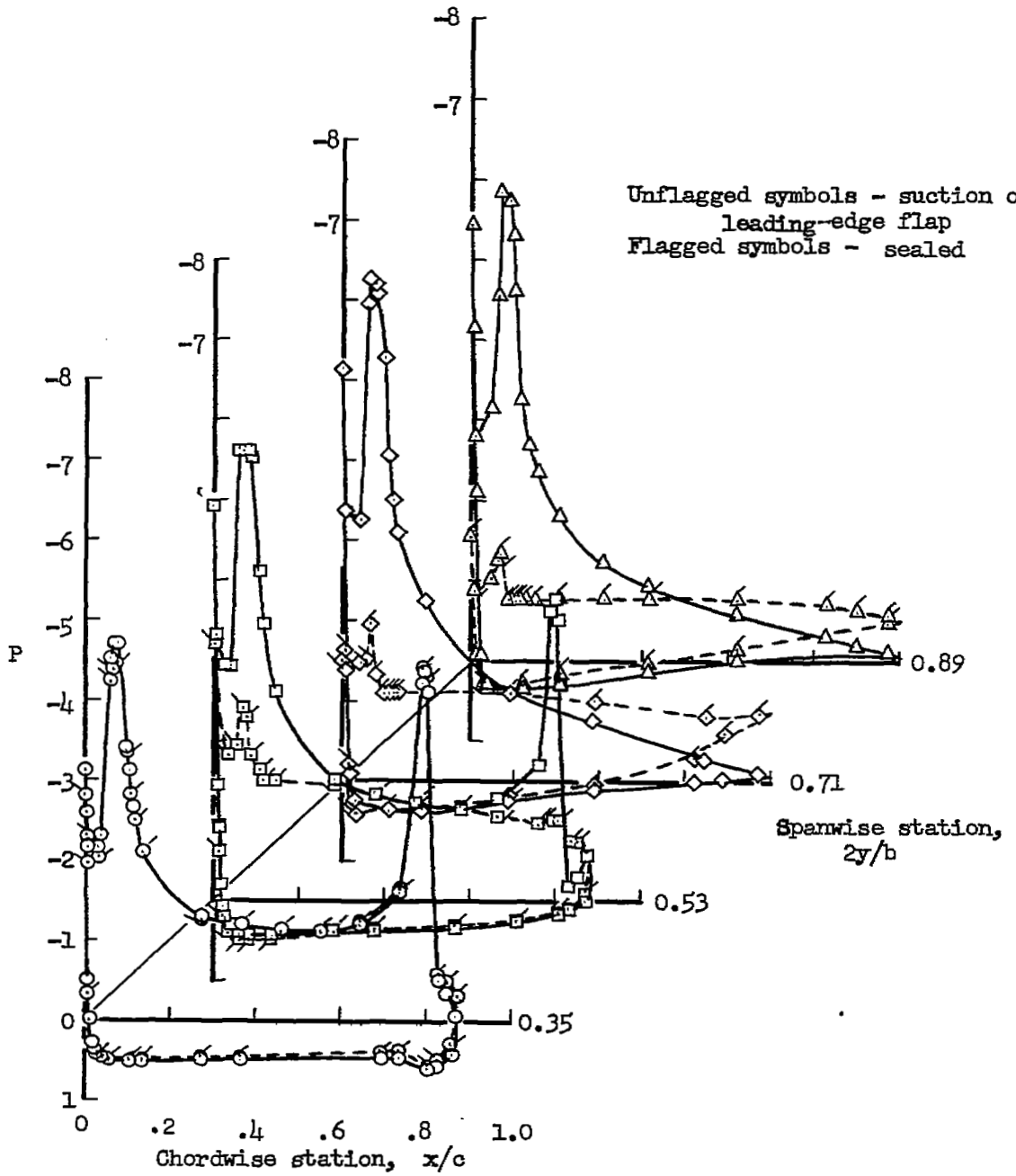

(c) $\alpha = 17.2^{\circ}$

Figure 23.- Continued.

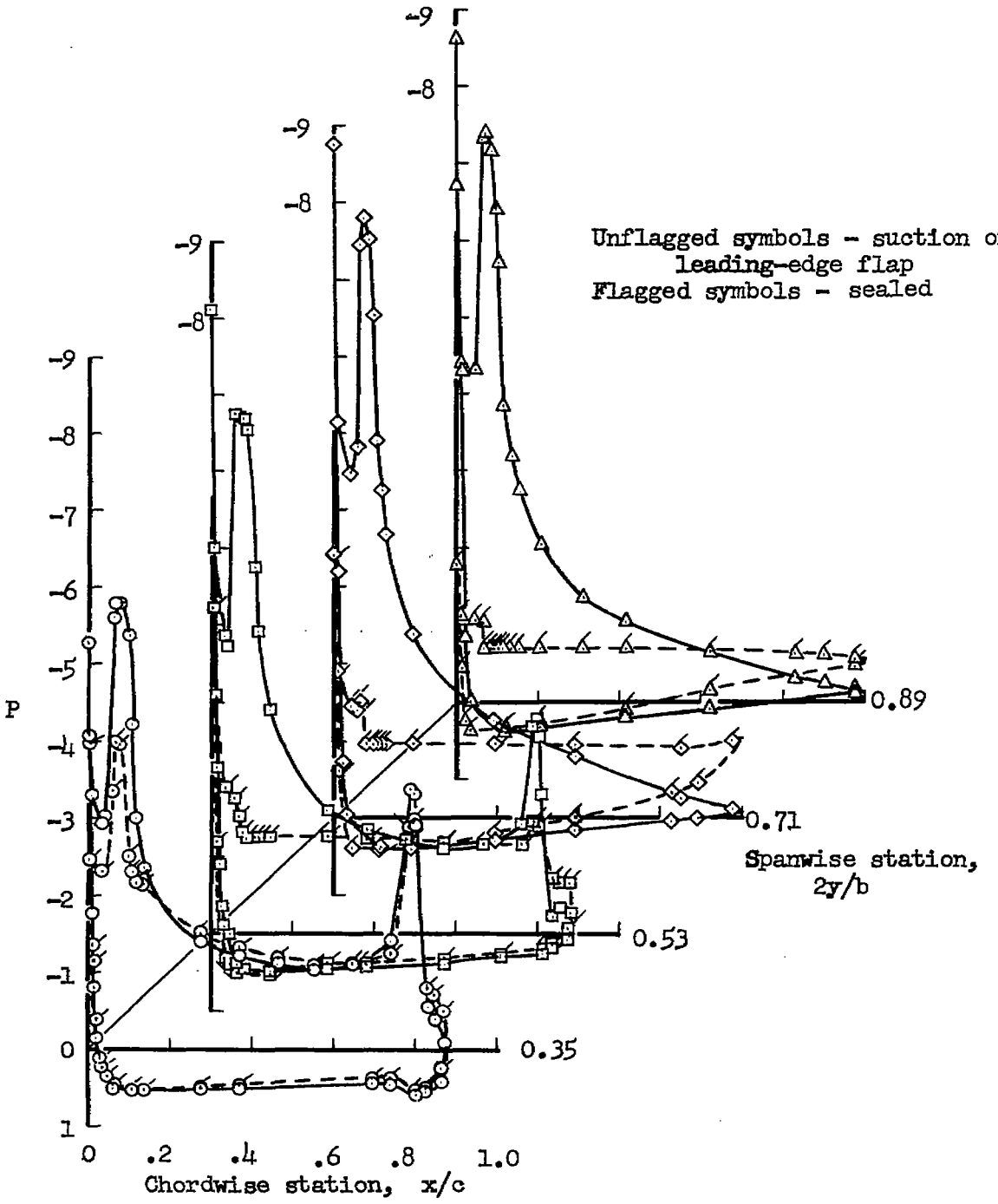

(d) $\alpha = 21.3^{\circ}$

Figure 23.- Continued.

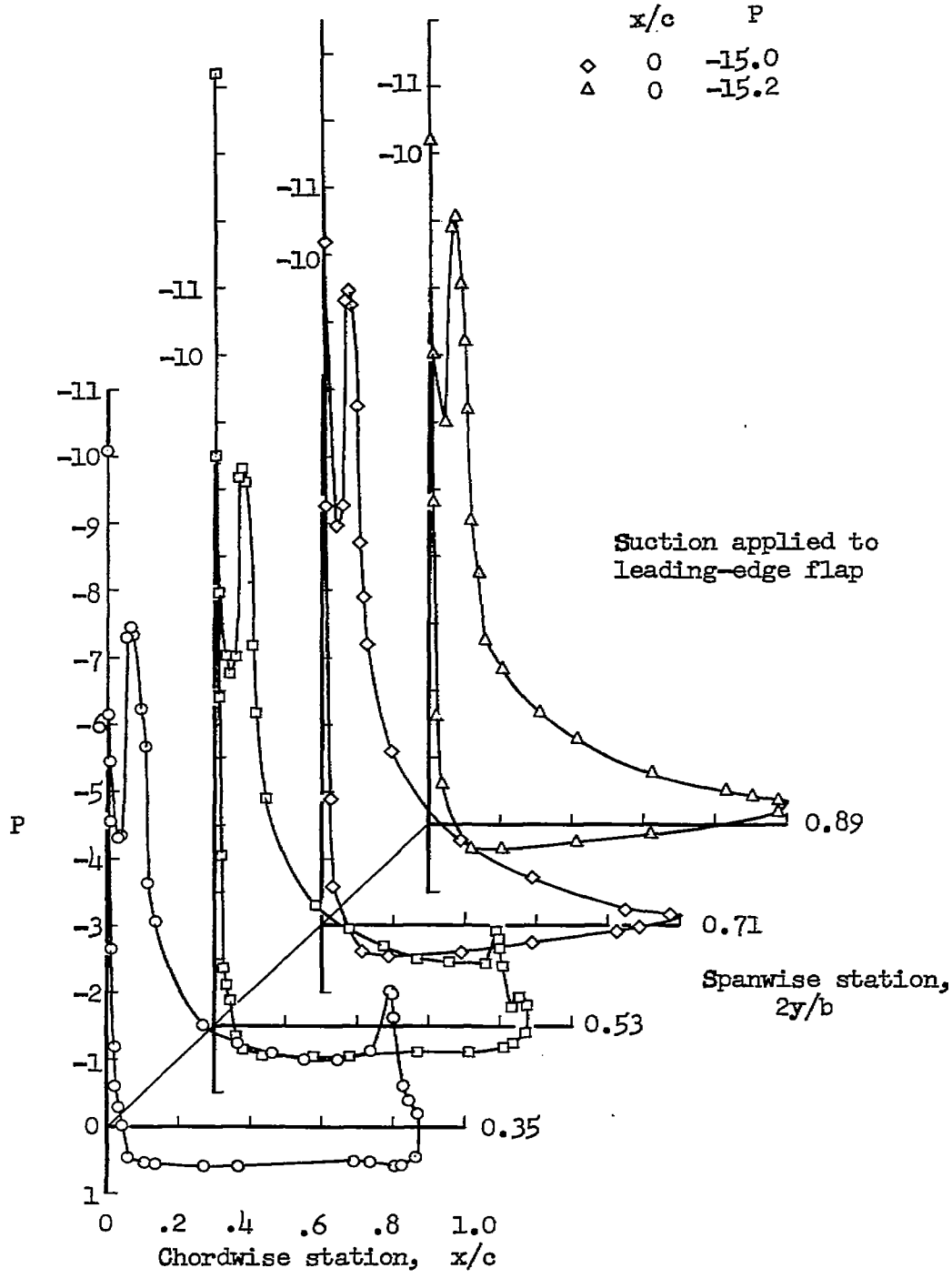

(e) $\alpha = 27.5^{\circ}$

Figure 23.- Continued.

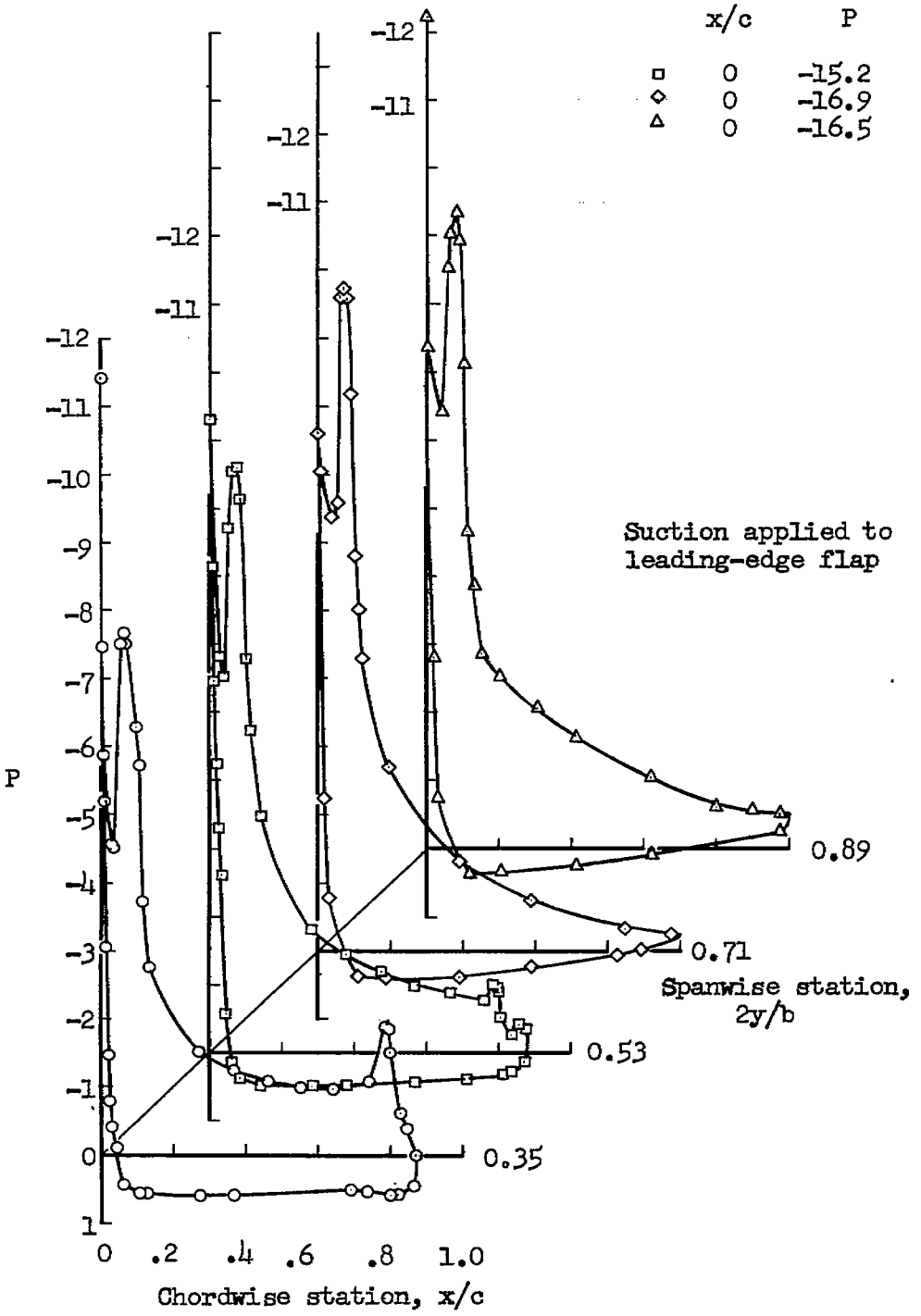

(f) $\alpha = 28.5^{\circ}$

Figure 23.- Continued.

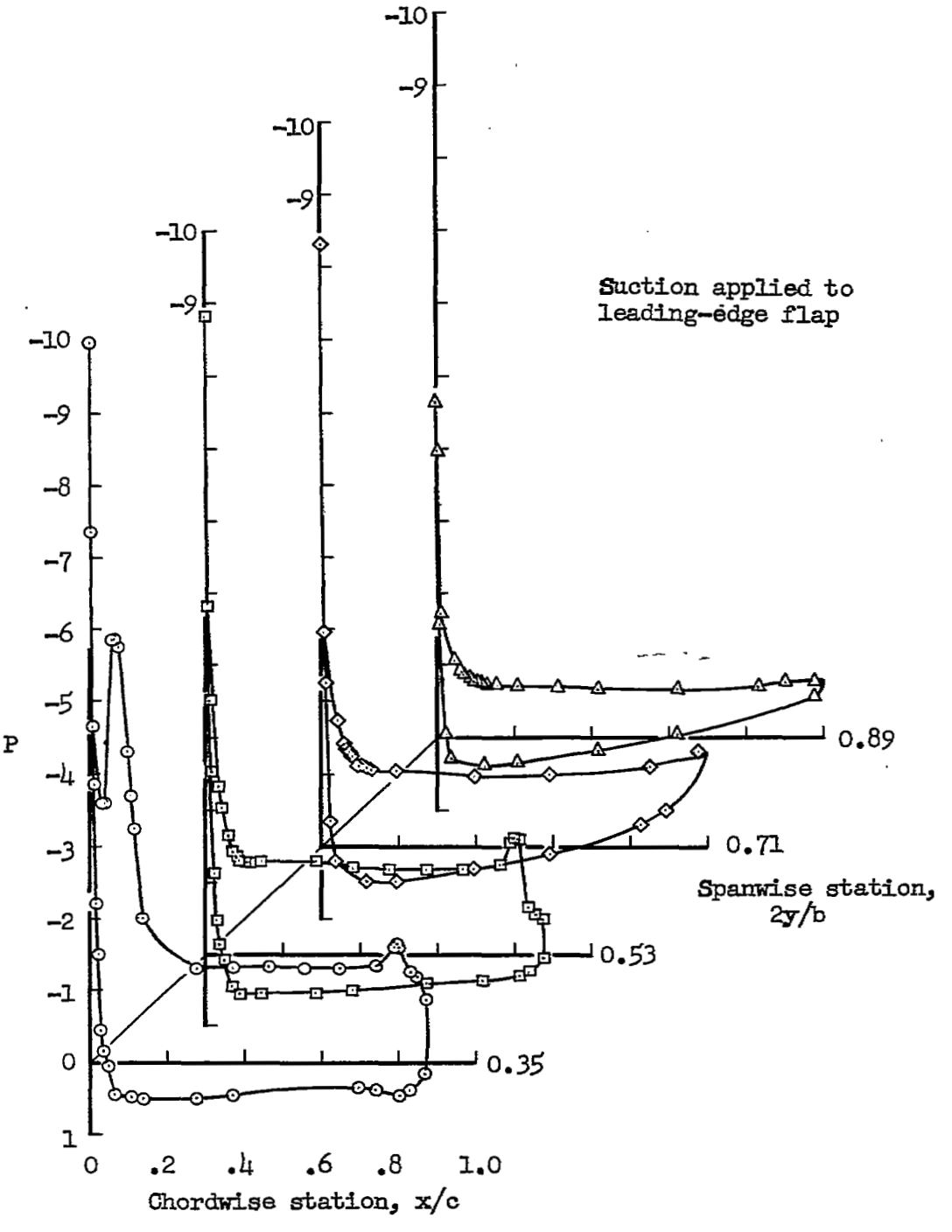

(g) $\alpha = 29.1^{\circ}$

Figure 23.- Concluded.

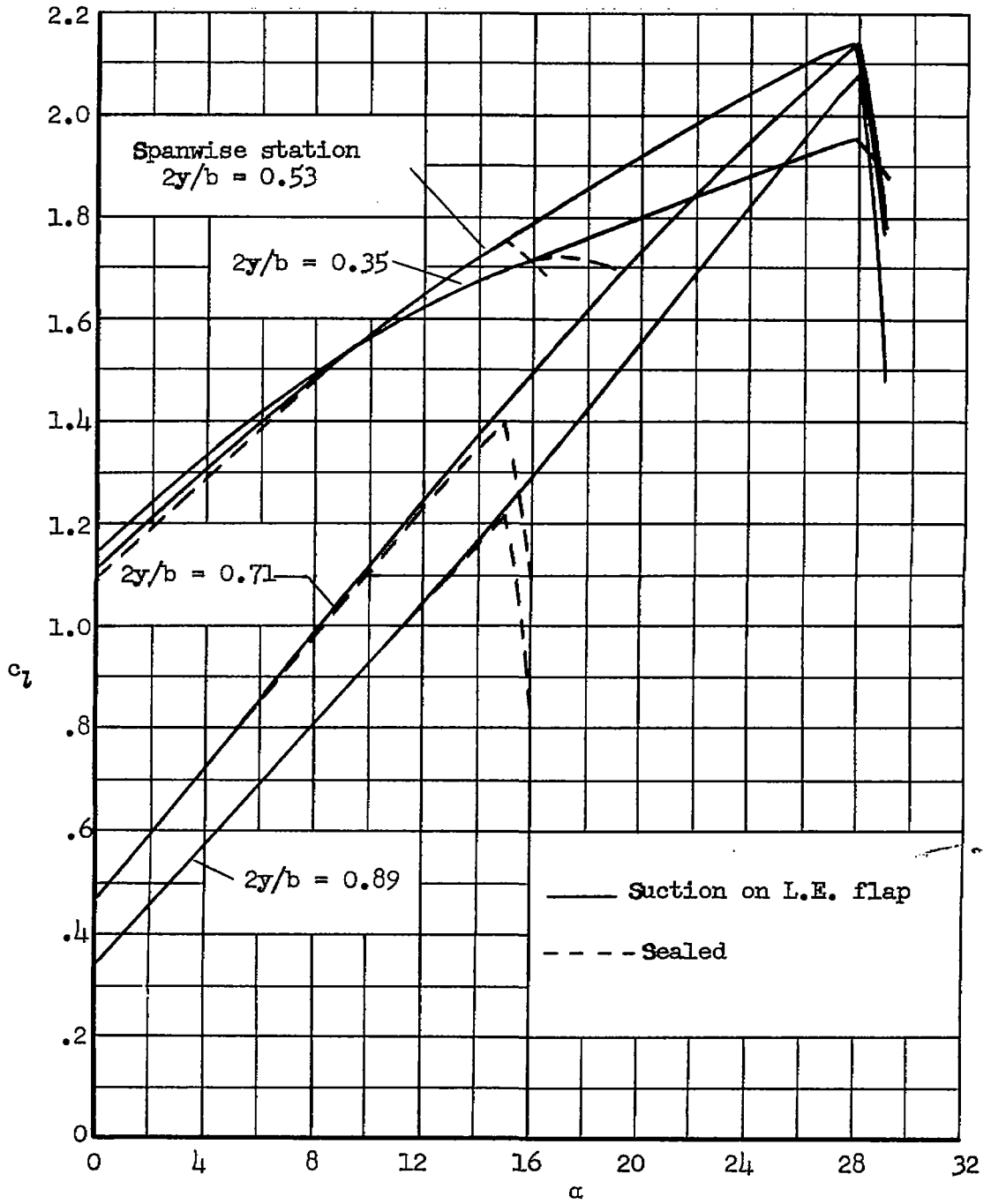

Figure 24.- Variation of section lift coefficient with angle of attack; $\delta_F = 66^\circ$, $\eta_F = 0.16$ to 0.50 with suction, $\delta_N = 40^\circ$, U = 156 ft/sec.

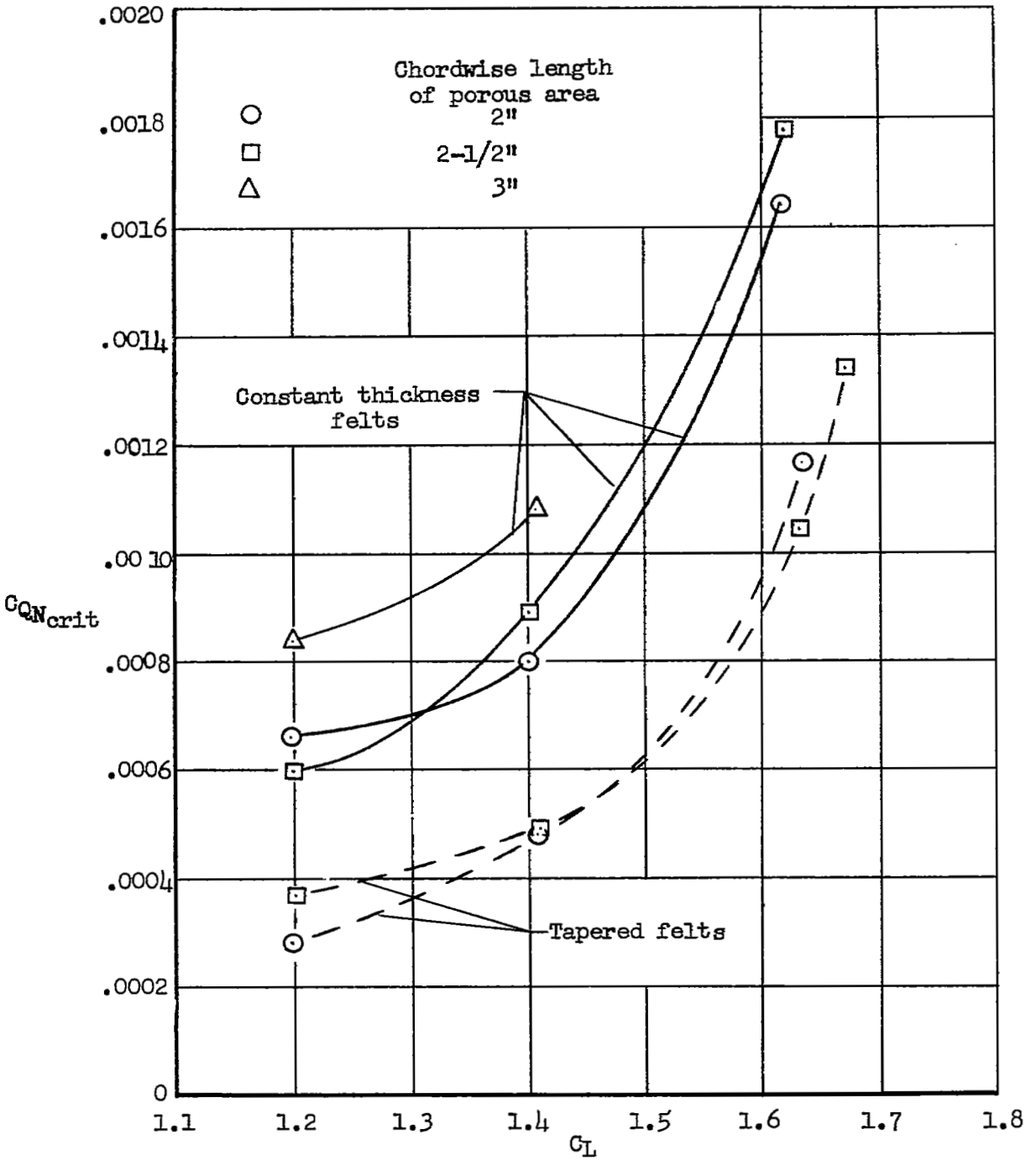

Figure 25.- Effect of porous area extent and design on critical flow coefficients for leading-edge flap; $\delta_F = 0^\circ$, U = 156 ft/sec.

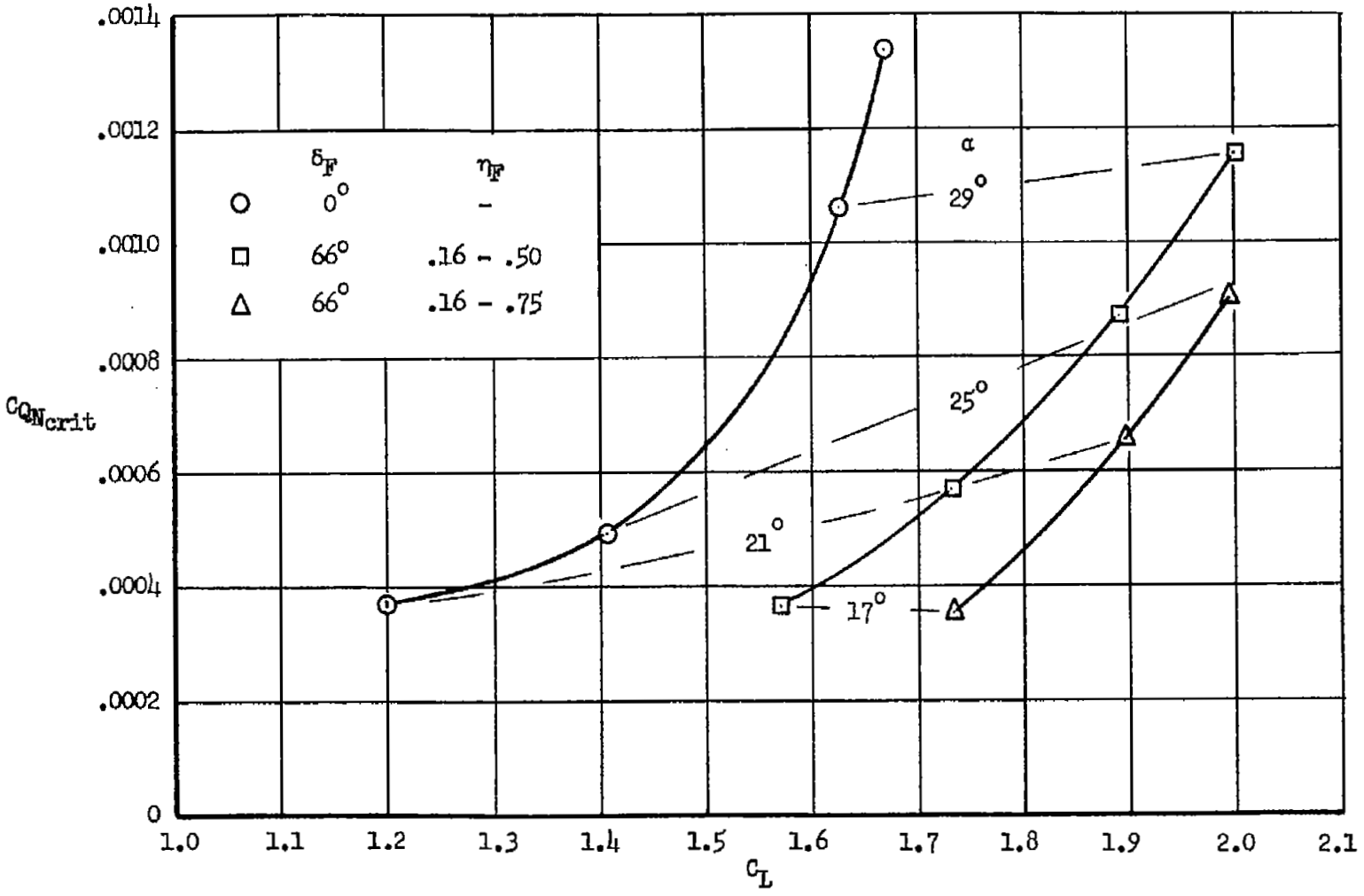

Figure 26.- Variation of flow coefficient with lift coefficient for the leading-edge flap; U = 156 ft/sec, tapered felts in leading-edge flap with 2-1/2-inch chordwise length of porous opening.

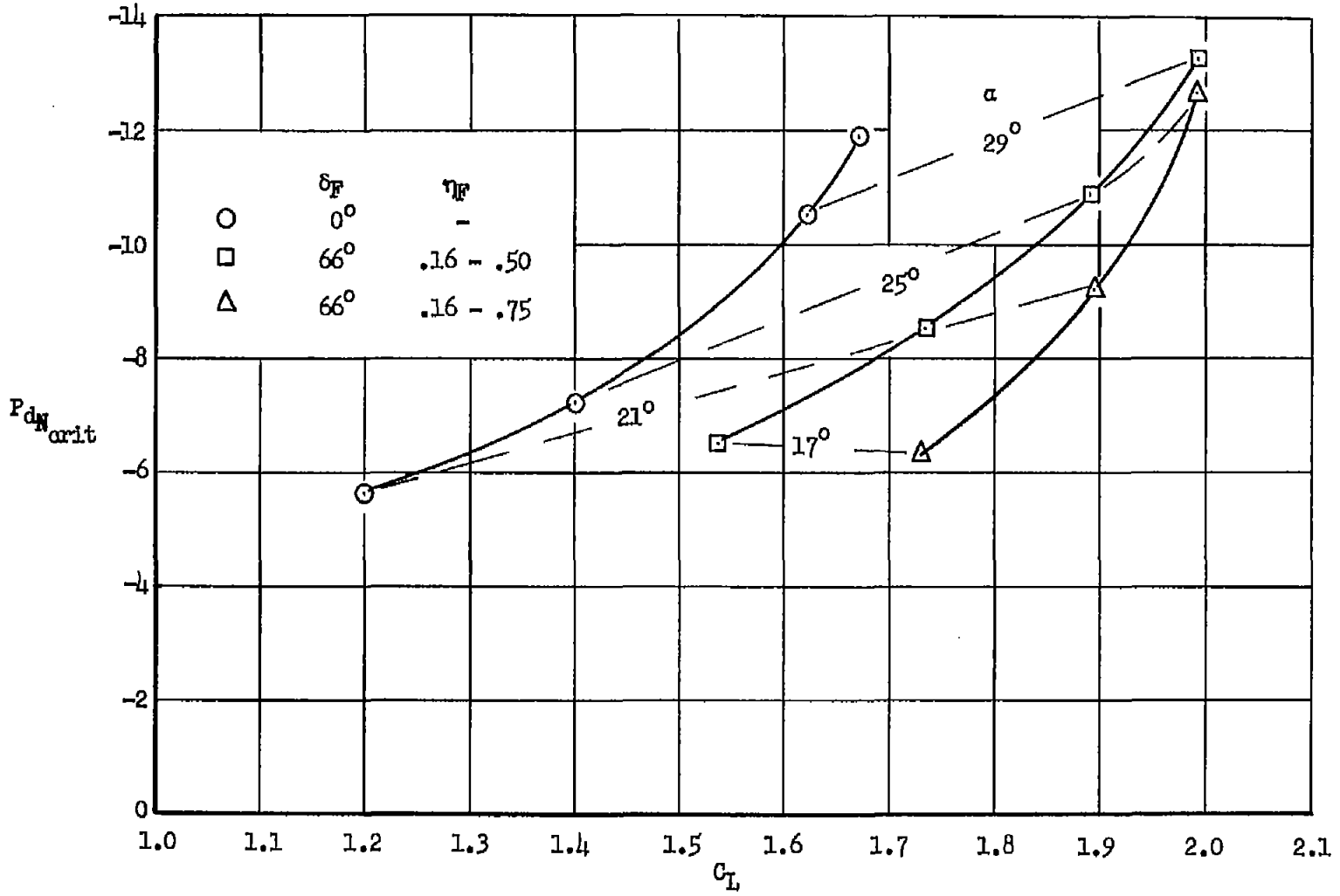

Figure 27.- Variation of duct pressure coefficient with lift coefficient for the leading-edge flap; U = 156 ft/sec, tapered felts in leading-edge flap with 2-1/2-inch chordwise extent of porous opening.

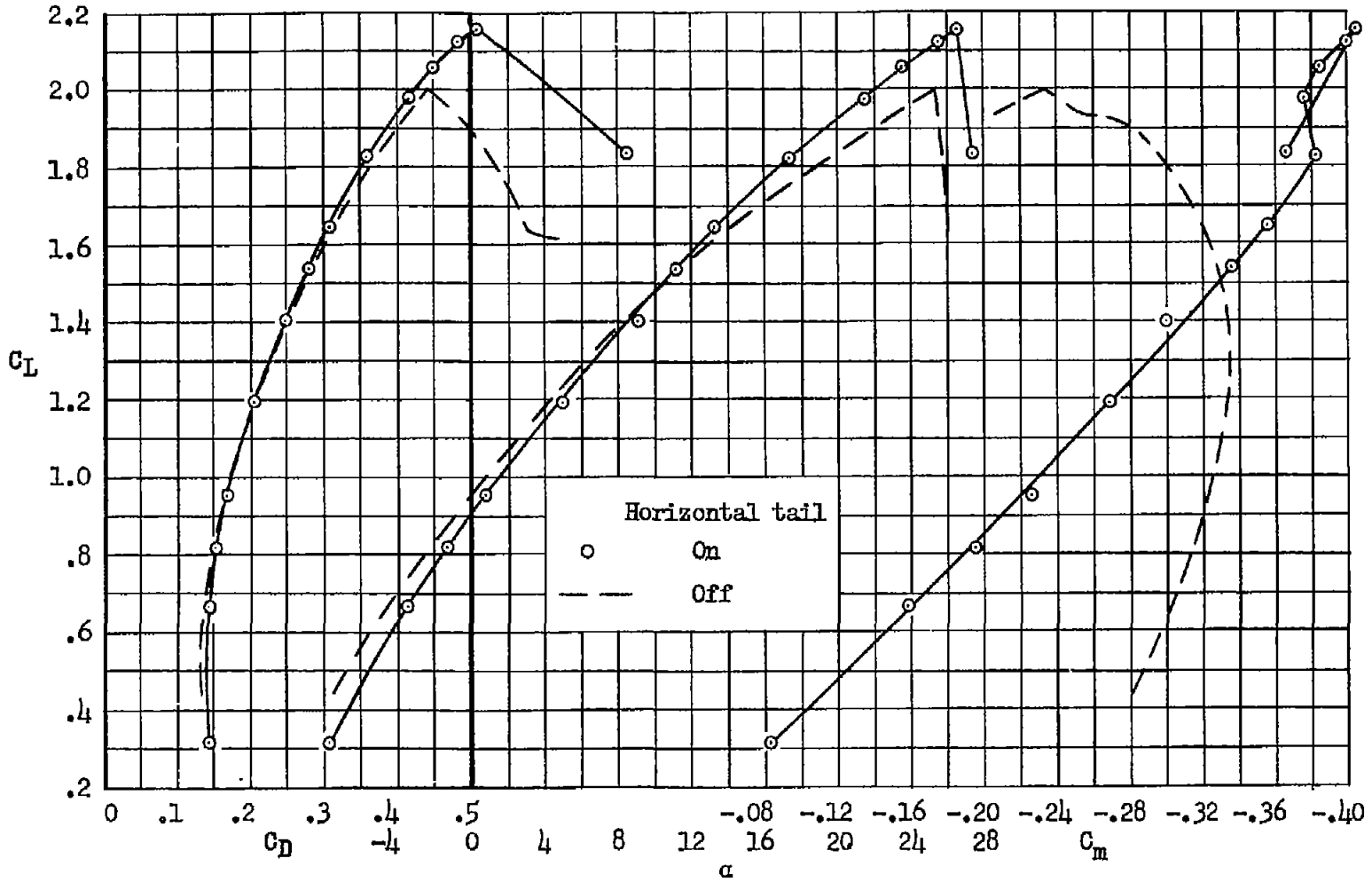

Figure 28.- Longitudinal characteristics of the model with suction applied to the 40° nose flap and to the 66° trailing-edge flap; η_p = 0.16 to 0.75, U = 156 ft/sec.